Synthesis of non-toxic colloidal silicon quantum dots and further optoelectronic device application

by

Jun Wang

A thesis

presented to the University of Waterloo

in fulfillment of the

thesis requirement for the degree of

Master of Applied Science

in

Electrical and Computer Engineering

Waterloo, Ontario, Canada, 2022

Author’s Declaration

I hereby declare that I am the sole author of this thesis. This is a true copy of the thesis, including any required final revisions, as accepted by my examiners.

I understand that my thesis may be made electronically available to the public.

Abstract

The promising electric and optical properties lead to the wide application of zero-dimensional quantum dots (QDs) in optoelectronic devices, such as quantum dots, light-emitting diodes (QLEDs), quantum dots-based solar cells, and photodetectors. The high light absorption and tunable light emission contribute to emerging QDs to push the energy structure transform towards a more sustainable direction. Si quantum dots (Si QDs) has the advantages of low toxicity and abundant raw materials compared to the traditional toxic Cd-based QDs, which are more sustainable and attract significant interest. Substantial development for the QDs stability and structure towards the optoelectronic application has been achieved these years. This thesis developed a modified low-temperature bottom-up silicon quantum dots (Si QDs) synthesis method with precursor AEAPTMS and green reductant L-AA. High luminescence and water-stable Si QDs were obtained, which emitted bright blue-green color under a UV lamp. Purification methods, including dialysis, filtration, and centrifuge, were employed to remove the impurities and restrain the QDs aggregation.

Afterward, to improve the applicability of Si QDs on photodetector devices, a solution-based ligand exchange process with 3-Mercaptopropionic acid (MPA) as the new ligand was investigated. Subsequently, the hydrocarbon chain was substituted by the shorter thiol ligand from MPA successfully. The ligand exchange Si QDs showed excellent photoluminescence emission intensity and remarkable water/ethanol stability. In addition, the lifetime of the Si-QDs increased by more than 20% and 45% compared to the non-ligand exchange ones. Besides, shorter MPA-ligand passivated Si QDs show fewer defects and better carrier transportability than the original QDs, which is more suitable for optoelectronic device.

Further, the manufactured MPA-Si QDs were incorporated as the light-harvesting layer in the planar ITO/ Si QDs/ Ag photodetector device. To improve the carrier separation, employ PEDOT: PSS as the hole transport layer. MPA-Si QDs showed a more excellent on-off ratio than the original Si QDs due to the less carrier transfer hindrance and the energy transfer from the mid-gap state, which also proves the necessity of the ligand exchange process.

Acknowledgments

First, I would like to express my highest appreciation for the help and support from my supervisor, Dr. Siva Sivoththaman; I am grateful for his guidance and instruction. Under his mentorship, I acknowledge the research's meaning and attitude. Thanks for everything you provide. It’s a great honor to work in your research group under your guidance. I would also thank the lab members from the Center for Advanced Photovoltaics and Display System (CAPDS) lab; this collaborative and encouraging environment helped me improve myself better. I would especially thank Dr. Hrilina Ghosh, you mentored me and provided detailed suggestions during my master's journey, and you are very responsible for the lab running. In addition, Dr. Fangyan Sun, thank you for your advice and help during the research project, and I will never forget the happy time we spent together. Dr. Bahareh Sadeghimakki and Dr. Roohen S. Tarighat, thank you for your insight and great advice. I would also like to thank my colleagues Jacob Brunning and Yizun Wang for their suggestions during the research. I would cherish the friendship we have. Next, I appreciate the help and encouragement from my friends. Thank you all for the accompany.

I would also like to acknowledge the external reader committees, Professor Hany Aziz and Professor Bo Cui. Thanks for your time and constructive feedbacks.

Last but not least, thanks to my parents, Hong Zhu and Jiangong Wang, your countless sacrifice made me pursue my dream and broaden my horizons. I appreciate the love, the help, the mentoring, and the support you give me. I love you.

Table of Contents

List of Figures

List of Tables

1. Introduction and motivations

1.1 Advanced solar energy and photodetector

Nowadays, global warming exacerbates the problem that humans need to solve. Due to the growth of energy demands, many fossil fuels burnt produce vast quantities of greenhouse gas emissions. As a result, frequent severe weather and more glaciers shrink. Several renewable energy sources, including winds, water, sunlight, waves, and biomass, are employed to generate electricity To curd the rapid global temperature increase. The advanced photovoltaic system plays a significant role in power generation; the solar panel converts light energy to electrical energy[1]. Photovoltaics devices would contribute to reducing 21% CO_2 emissions by 4.9 gigatons (GT). The solar system owns the capability to generate more significant than 25% of electricity demands in 2050 [2]. In addition, photovoltaic devices have excellent properties, such as low cost, abundant energy sources, and high efficiency. This remarkable performance of photovoltaic devices leads to solar energy becoming one promising and dependable energy source compared to other renewable energy. Price, stability, lifetime, safety, and efficiency are the dominant aspects affecting solar cell operation. Therefore, researchers keep working on developing emitter materials and solar cell structures to optimize efficiency and reduce cost.

Up to now, there are typically three major generations of solar cells that have been elaborately studied and reported, which includes the first-generation wafer-based solar cell, the second-generation thin-film solar cell, and the emerging third generation. However, the Shockley-Queisser effect limits the first generation single-junction silicon solar cell efficiency, which is 31% in the ideal situation[3]. Then researchers focus on investigating the device structure and material to break through the limit. One of the excellent third-generation emerging solar cells is the quantum dots-based solar cell, which has rapid development and increased its efficiency from 2% to 18.1%

in 10 years[4]. Shortly, it is expected to become a remarkable alternative to surpassing crystalline silicon solar cells.

Quantum dots (QDs) synthesis is based on notable nanotechnology, which significantly promotes energy innovation in sustainable and environmentally friendly directions[5]. Compared to bulk semiconductors, zero-dimensional material QDs have promising optical and electric properties, which originate from the size-dependent quantum confinement effect and attract researchers' particular interest [6]. As shown in Fig.1-1, compared to the dense conduction band and valence band in the bulk semiconductor, there are numerous discrete energy states in QDs depending on the size[7]. Besides the tunable band gap, strong light absorption, high photoluminescence(PL), and surface-to-volume ratio, these distinguished capabilities all contribute QDs becoming one competitive light-absorption material in optoelectronic device applications [8]. With the tunable band gap and high sensitivity to light, QDs are suitable to apply to the photodetector device, and comprehensive light detection can range from ultraviolet to mid-infrared region[6].

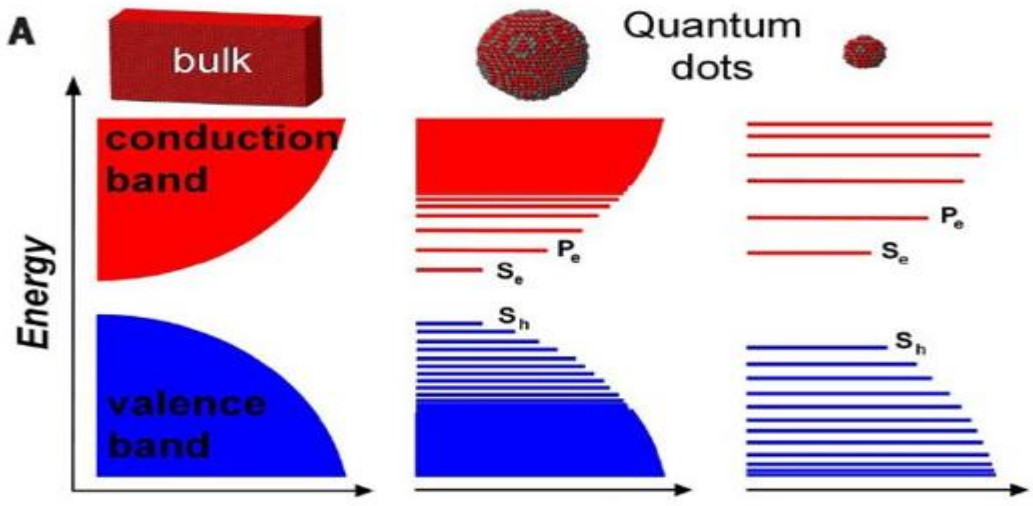

Figure 2-1 electronic states in quantum dots and bulk material[7].

1.2 Wide applications of quantum dots

In addition to the solar cell and photodetector application, non/low-toxic QDs such as Ag_2S QDs, and Si QDs can also be applied to cell-imaging, bio-labeling, and bio-medicine[9][10][11]. Based on the static quenching mechanism, the Si-QDs biosensor showed the fast detection of Hg^{2+} and thiols, which can be applied to labeling glutathione in tumors [12]. In addition, with high quantum photoluminescence and long penetration length in vivo, Ag_2S QDs with comparable protein sizes are suitable for bio-imaging[13]. Moreover, the protein residue in the fingerprint can interact with positively charged CdTe QDs, and the electrostatic force between positive-QDs and negative charge protein will label the QDs on the fingerprint, which illustrates the fingerprint texture and can be further used for forensic application[14]. Besides, high PL emission and pure color emitting motivate QDs-based light emitting diodes (QLEDs) devices of great interest. Further treatment can extend the lifetime and stability, and proper encapsulation can help inorganic perovskite-based QDs emit ideal white light steadily under low operation current [15]. In summary, the wide applications of the QDs play a vital role in biometric identification and new energy innovation.

1.3 The motivation for this research

1.3.1 Developing the synthesis of non-toxic silicon quantum dots

Cadmium (Cd) and lead (Pb) based quantum dots are the most common materials due to their narrow emission and excellent stability. These properties lead to their wide applications in solar cells and QLEDs. But the toxicity violates the safety rule and limits their commercial scale-up application[16]. Thus, investigating less-toxic quantum dots is becoming an urgent scientific demand. Compared to the bulk semiconductor silicon, nanometer-sized Si QDs own the quantum confinement effect and tunable bandgap, which is of particular interest[17]. In addition, the less

toxic, high photoluminescence and cost-effectiveness make the Si QDs a competitive substitute for highly toxic Cd-based QDs.

From the synthesis method aspect, traditional electrochemical etching, template synthesis, and plasma synthesis methods need high energy/corrosive acid (hydrofluoric acid) and violate sustainability. The solution-based synthesis method uses relatively low temperature, facile set-up, and mild acid, which is more cost-effective and sustainable[18]. Thus, the motivation of this research is to develop high photoluminescence Si QDs in a sustainable method.

1.3.2 Optimizing the silicon quantum dots and optoelectronic device fabrication

The light emissions and carrier transport play a significant role in applying the QDs on the optoelectronic device. Nowadays, the tendency to implement QDs as the light-absorbing layer in photodetector applications has become more prevalent. The ligand and QDs film polarity play critical roles in photodetector performance; unsuitable ligand and polarity will lead to poor film adhesion and hinder the free carrier transport, which confines the response of the device[20]. Meanwhile, the length of the ligand needs to be sufficient to provide excellent dispersibility[21]. Thus, to obtain excellent solubility and desirable ligand length, the choice of the reactants and ligand are essential to pay attention to and is still under investigation.

In addition, the stability of Si QDs is another emerging problem researchers face. Hydride-terminated QDs are apt to be oxidized when exposed to moisture or oxygen and further affect their optical and electric properties[19]. Microencapsulation and ligand exchange processes are the mainstream methods to improve material stability [22]. Then developing the stability of synthesized Si QDs for optoelectronic device application via ligand exchange process is also one of the primary research motivations. In device fabrication, functional layers coating will introduce

ambiguities for the device's performance. Then the device fabrication parameters and active layer chosen also need to be explored.

1.4 Research objectives

Research objectives include bottom-up Si QDs synthesis, QDs optimization and characterization, QDs ligand exchange with MPA, and Si QDs-based photodetector device characterization fabrication.

Objectives 1: Develop low-temperature bottom-up Si QDs synthesis, exhausting research was executed on obtaining the high photoluminescence optimal QDs, reaction temperature and further purification effect is thoroughly investigated and characterized.

Objective 2: Develop the Si QDs with the ligand exchange process. For photodetector device applications, Si QDs used as the light-harvesting layer. The light absorption ability and carrier transportability is developed by replacing the long alkyl ligands with 3-Mercaptopropionic acid (MPA).

Objective 3: Develop and fabricate the Si QDs-based photodetector; the light current examines the planar fabricated device performance to dark current ratio.

1.5 Organization of this thesis

This thesis primarily focuses on the synthesis of Si QDs and further development, including exploring the optimal reaction condition and purifying the Si QDs, modifying the Si QDs via the ligand exchange process, and further applying the Si QDs on the photodetector.

Chapter one introduces the QDs' role in photovoltaic and photodetector applications and states the research motivation.

Chapter two presents the literature review, which mainly focuses on the Si QDs synthesis method, ligand effect on the Si QDs' tunable color emission and solubility, and Si QDs based optoelectronic device performance.

Chapter three states the facile and environmental-friendly bottom-up method to synthesize high photoluminescent Si QDs. Using silanes as the silicon precursor, L-ascorbic acid (L-AA) acted as the reactant and applied mild reaction conditions to carry out the reaction. The structure of Si QDs and reaction conditions were investigated. Various characterization results were used to analyze the synthesized Si-QDs.

Chapter four proposes a solution-based ligand exchange method to facilitate the photodetector device. 3-Mercaptopropionic acid (MPA) is added to finalize the ligand exchange process, which substitutes the long carbon side chain and passivates the QDs surface. The thiol-terminated structure extends more than 20% lifetime of QDs and promotes the photodetector response. The Fourier transform infrared spectroscopy (FT-IR), and optical photoluminescence measurement demonstrates the ligand exchange. This facile stepwise synthesis material can turn into a great replacement for toxic Cd-based QDs.

Chapter five mainly focuses on investigating the device fabrication parameters. The performance comparison of MPA ligand exchange QDs and original Si QDs was carried out, and the I-V measurement characterized the fabricated devices. The remarkable improvements of MPA-Si QDs' light current to dark current ratio were obtained compared to the weak light response of the non-ligand exchange Si QDs.

Chapter six summarizes the research discovery results and states the outlook for Si QDs and QDs-based optoelectronic devices.

2. Literature review

2.1 Synthesis of silicon quantum dots

The prominent silicon quantum dots synthetic methods are divided into top-down and bottom-up approaches. Top-down processes usually employ macroscopic objects via physical or chemical methods to achieve a nanometer/micrometer range. The rate is dominant by Moore's law and relies on physical techniques, such as electron beam lithography and laser[23]. Bottom-up is based on the self-assembly process, which usually starts from the molecular-level silicon precursor and grows to the nanometer-sized quantum dots[24].

Top-down methods mainly consist of chemical/electrochemical etching, laser-ablation, and Si QDs can be obtained from silicon wafers directly. The first electrochemical-etching Si QDs was achieved by Sailor et al. in 1991, silicon wafer immersed in diluted HF acid with platinum as the counter electrode, followed by ultrasound processing, and luminescent colloidal Si QDs were prepared successfully[25]. Chemical etching is extensively investigated with easy access to the raw material and facile setup. Afterward, the size-tunable was improved by Jeong et al. via control of the HF and nitric acid etching time, and silicon nanopowder was etched, assisted with sonication, and further terminated the product by the 1-octadecene (ODE). Si QDs emission wavelength can tune from 404nm to 507nm[26]. A physical method such as laser-ablation QDs is gained via laser irradiation on the Si wafer in a helium environment; the deposited QDs film can further be detached and dissolved in the solvent[27]. The advantages of the most top-down method include abundant silicon sources and fewer impurities. However, the top-down physical approaches highly relied on the exactitude instrument, and the chemical top-down method essential demand on the corrosive HF acid, which is costly and violates sustainability. Thus, high throughput and scale-up production are still under-solved.

Bottom-up methods principally consist of silicon-precursor reduction and the Zintl salt reaction. Kauzlarich et al. firstly carried out the low-temperature synthesized Si nanoparticles(NPs) by reducing silicon tetrachloride($SiCl_4$) with sodium naphthalide. Si NPs (5.2nm$\pm$1.9nm) with blue light emission were obtained[28]. Afterward, monodispersed Si QDs were obtained by Tilley et al. by employing tetraoctyl ammonium bride (TOAB) as the surfactant to restrict the final growth size of the QDs, and narrow distribution(1.8 $\pm$0.2nm) was achieved[29]. Further solution-based Si QDs with tunable size were achieved by Mohammed et al.. Hydrogen-terminated Si QDs were synthesized via reacting $SiCl_4$ with lithium aluminum hydride ($LiAlH_4$) and TOAB. Then functionalized Si QDs with 9-vinyl pyrene, 1-vinyl pyrene, and 3-vinyl perylene to enhance the stability and quantum yield. As a result, a tunable emission from 358nm to 515nm was obtained and can be applied in the bio-imaging field[30]. Another popular bottom-up method is the zintl salts reaction. Metathesis reaction can happen between high ionic reactivity zintl salts (Si_xMe_y, Me=Na, K, Mg) and Silicon halide or bromine at low temperature due to their specific crystal chemistry, and the reaction is driven by the thermal process and yield Si QDs. Chung et al. first demonstrated the metathesis reaction between the Mg_2Si and $SiCl_4$, and a chloride terminated blue-emission silicon cluster was obtained[31]. The effortless operation and cost-effectiveness drove the extensively researched of this method. However, this method still suffers from the low yield issue. Atkins et al. carried out the microwave-assisted synthesis reaction between Na_4Si_4 and ammonia bromide. This one-pot method obtained the Si QDs with 2-3nm diameter and can enhance the yield effectively with microwave assistance [32].

From the perspective of sustainable and green synthesis, bottom-up synthesis uses mild reaction conditions and less-toxic reactants, which is fit for large-scale production.

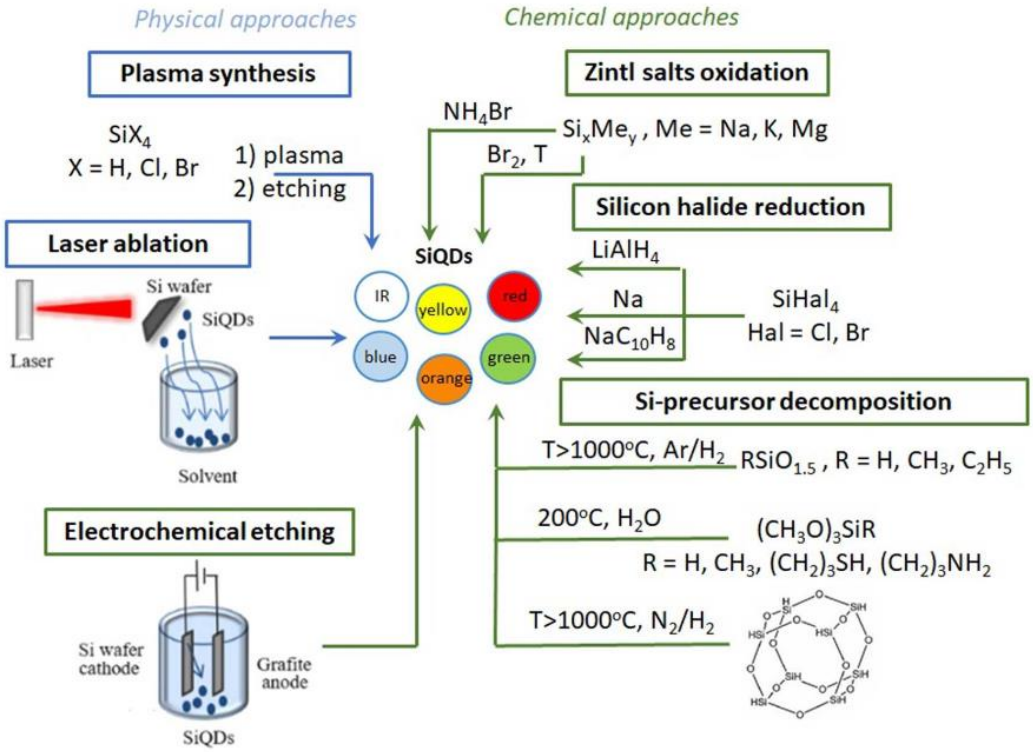

Figure 2-1. silicon quantum dots synthesis methods[33].

2.2 Silicon quantum dots ligand exchange/surface passivation

Hydride-terminated Si QDs suffer from the stability of Si QDs is also one emerging problem that researchers are facing. Hydride-terminated QDs are apt to be oxidized when exposed to moisture or air and further affect their optical and electric properties[19]. To improve material stability, QDs can be modified by microencapsulation and ligand exchange methods [22]. The dangling bonds on the surface can be passivated by chemical bonding new ligands, which restrain the undesirable non-radiative recombination and increase the PL intensity[7]. In addition, the ligand attached can modify the solvent dispersibility of the QDs.

Meanwhile, ligand exchange is also one promising method to achieve size turnability and alter the Si QDs emission color for various applications through modifying the energy state levels.

Kang et al. took advantage of the easy oxidation of the H-terminated Si QDs surface by controlling the hydrogen peroxide oxidation time to achieve tunable emission of water-soluble Si QDs. As shown in Fig2-2, the results indicated longer oxidation time results in QDs core size shrinking and emitting seven colors, this tunable color emissions are promising for bio-labeling application[34]. Nakamura et al. used the top-down method to synthesize Si QDs with p-type Si flake in 1-decene or ethyl 10-undecenoate; the QDs reacted with 1-decene showed good solvability in non-polar hexane due to the non-polar alkyl ligand attached on the QDs surface, as QDs synthesized in ethyl 10-undecenoate with ester-group attached dispersed well in polar solvent ethanol. This illustrates ligand changed the QDs dispersibility effectively [35]. Besides, the organic ligand passivation of the hydrogen attached to the Si flake via the hydrosilylation process improves the PL emission because alkyl bonds depress the non-radiative recombination[36][37]. Ghosh et al. stated the alkyl-terminated Si QDs could increase the PL quantum yield dramatically compared to the H-terminated Si QDs, the possible mechanism is the alkyl ligand behaves as support to restrain the lattice distortion, and the distorted H-Si QDs will suffer from the non-radiative recombination process[37]. H-terminated QDs surfaces are noticeably highly reactive, and alkene-terminated surfaces are less unreactive than alkyne-terminated ones. Highly stable ligands are not preferable when further the QDs surface functionalization for specific applications will be implemented[32].

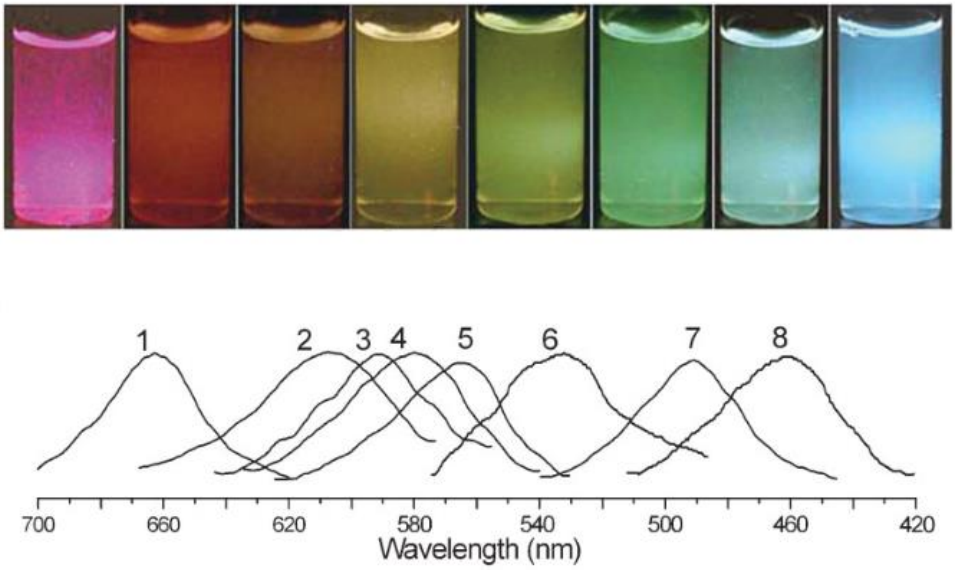

Figure 2-2. Photograph of tunable Si QDs and PL spectra after 0, 0.5, 1.5, 3.5, 6, 9, 14, 24h oxidation, respectively[34].

The stability of QDs is essential for long-term application, and ligand length will influence the carrier transport during the interface and functional layer. Yu et al. used 1-Dodecanethiol/ Dodecene as the vicarious surface functional group source to alter the hydride ligand attach on the Si-QDs, which improves the moisture stability of the material. But the long side chain is not perfect for the optoelectronic application due to the high energy barrier[38]. The electronic state overlap is less, and barrier height is higher in long-chain QDs, which will decrease the QDs film conductivity and hinder the free carrier transport during the device operation, also leading to poor response to light or external bias[39]. Xu et al. also researched the quantum dots ligand passivation effect, and they found the decyl-terminated QDs have better stability and can be incorporated into the LEDs; passivating the QDs surface can improve the LEDs' EQE effectively. But the device's performance was also limited by the insulation effect caused by the complex ligand; the usage of toxic solvent toluene is also against sustainability and environmental-friendly[40]. In addition,

poor QDs film coverage is a vital problem for the device efficiency. Zhong et al. demonstrated that MPA-ligand capping QDs can spread well and increase the QDs loading on the electrode, which enhance the QDs-based solar cell efficiency[41]. Recently, multistep passivation has been explored to passivate surface defects better. Sargent et al. developed a hybrid passivation process that passivates the lead sulfite (PbS) QDs surface with MPA and halide anions. MPA takes the place of the original long ligands. Small size halogen can cover the QDs surface trenches that MPA is unable to. This process validly removes the mid-gap traps and enhances carrier mobility in optoelectronic device applications [42]. The shorter MPA chain decreases the interdot distance, which increases the QDs packing densities and fastens the carrier transport. Huang et al. worked on the hybrid passivation with MPA and imported iodide anions to suppress the recombination loss, results indicated excessive iodide would restrain the QDs' light absorption, and the proper amount added can enhance the solar cell fill factor effectively[43]. Therefore the ligand exchange process is necessary to increase optoelectronic device performances [39].

2.3 Silicon quantum dot application in optoelectronic devices

Silicon quantum dots are a suitable candidate for non-toxic optoelectronic devices application with their high luminescence, tunable bandgap, and color emission. Ghosh et al. applied the high quantum yield alkyl-terminated Si QDs as the efficient emitters, transparent indium tin oxide (ITO) and aluminum were applied as the electrode. 40nm poly(3,4-ethylenedioxythiophene)-poly(styrenesulfonate) (PEDOT: PSS) as hole transfer layer (HTL) and 40nm 1,3,5-Tris(N-phentl-benzimidazole-2yl)(TPBi) acted as the electron transport layer(ETL), and the work function of PEDOT: PSS is suitable for the hole injection into Si QDs layer. Meanwhile, the deep highest occupied molecular orbital (HOMO) of TPBi can block the hole injection. External quantum efficiency (EQE) is one of LEDs' most critical performance properties. For this QDs-based LEDs,

the EQE results in red, deep-red and near-infrared were obtained as 0.2%, 0.23%, 0.22%, respectively[37]. The tunable light emission is promising for LEDs applications. However, the lower value of EQE still needs to be improved and may originate from the long ligand of 1-decene-capped Si QDs defects, leading to poor carrier transport and non-radiative recombination.

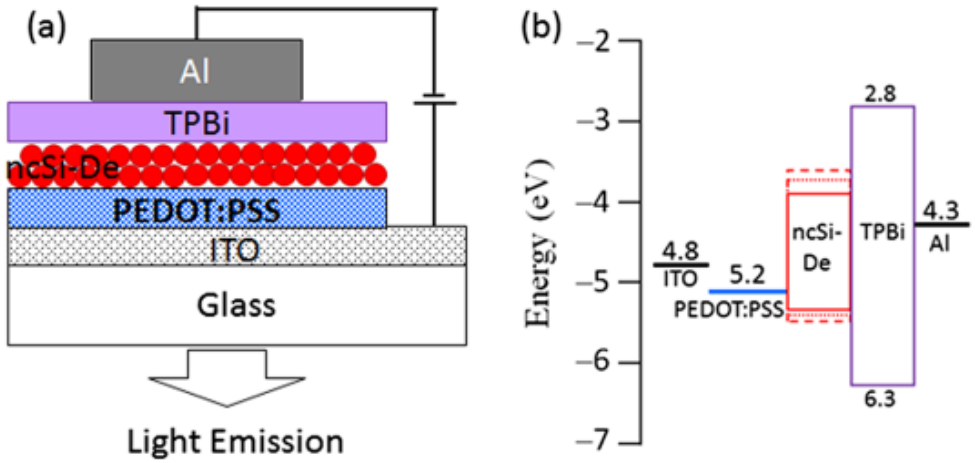

Figure 2-3(a) ligand exchange Si quantum dots based LEDs scheme (b) LEDs energy level under zero bias[37]

Liu et al. developed Octyl and Phenylpropyl capped Si QDs, and further QLEDs ligand effect on LEDs performance were investigated. PEDOT: PSS and zinc oxide (ZnO) were employed as the hole transport layer (HTL) and ETL. Si QDs with different ligands were utilized as the emitter material. PhPr-Si QDs showed higher PL intensity and longer lifetimes than Octyl-Si QDs due to fewer dangling bonds on the surface. The EQE for PhPr-Si QDs and Octyl-Si QDs were 1.1% and 6.2%,respectively[21]. The mechanism behind the significant difference in EQE is the electron transportability in PhPr-Si QDs is quite high compared to its hole transportation, which is due to the benzene ring being adapted in the electron transport. This property contributes to the

unbalance hole and electron injection in the QDs layer, resulting in electron leakage and lower EQE.

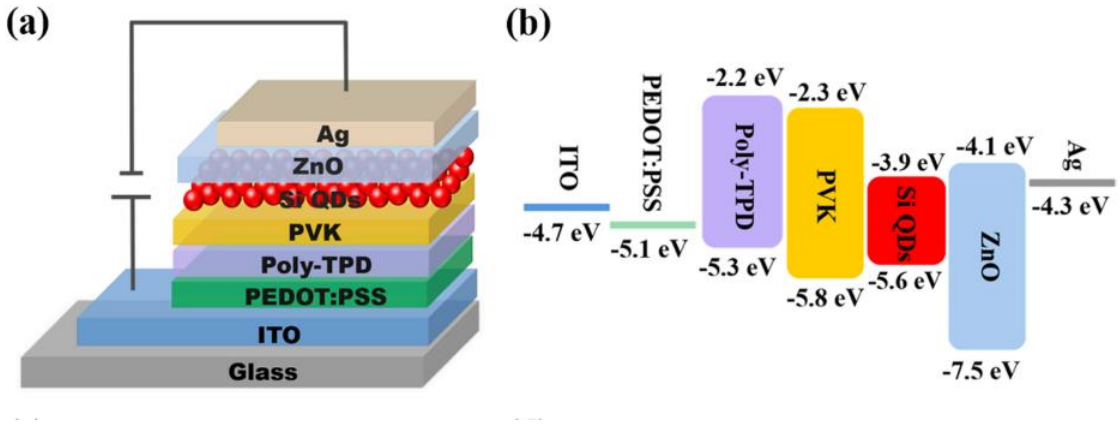

Figure 2-4(a) silicon quantum dots LEDs scheme (b) device energy diagram[21]

Besides the emitter application in LEDs, Si QDs can be applied as the light-absorbing layer in the photodetector. Yu et al. fabricated the photodetector by coupling Si QDs with graphene and forming the Schottky junction with Si. Si QDs layer can enhance the photocurrent validly through transferring charge to graphene and lowering the graphene Fermi level. The built-in potential increases afterward and promotes charge separation. In addition, Si QDs also boost the photodetector photon response of longer wavelength and sustain the reflectance of the light due to Si QDs' excellent light absorption ability and scattering. The fabricated device showed extremely fast photo response in $3*10^{-7}$s, and Si QDs raised the detection limit efficiently. A broad detection range from 350nm to 900nm is promising to be applied for the bioimaging area.

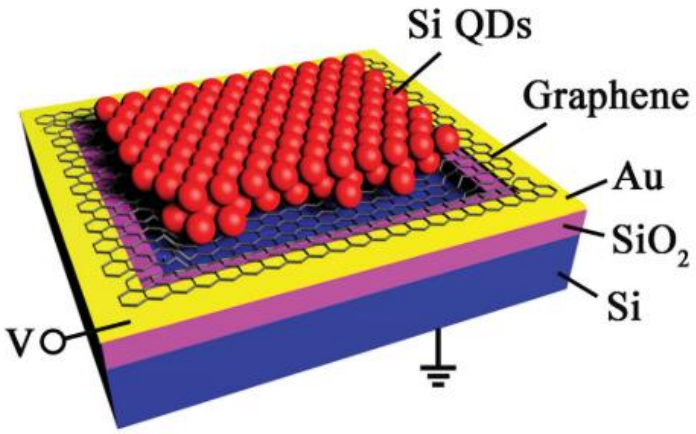

Figure 2-5 Silicon quantum dots coupled with graphene photodetector [44].

3. Silicon Quantum Dots synthesis and characterization

Safety, sustainability, and cost-effectiveness are the primary requirements for large-scale production. Compared to top-down methods' low yield and harsh synthesis conditions, bottom-up methods are more controllable and more applicable for scale-up production. Due to the high toxicity of Pb-based and Cd-based QDs, the demand for developing non-toxic Si QDs becomes paramount. Thus, this work presents one facile and environmentally-friendly method to synthesize high photoluminescent Si-QDs. Meanwhile, propose a facile ligand exchange method to facilitate the photodetector device. Use [3-(2-Aminoethylamino)propyl]trimethoxysilane (AEAPTMS) $(CH_3O)_3$-Si-$(CH_2)_3NHCH_2CH_2NH_2$ as the silicon precursor. L-ascorbic acid (L-AA) acts as the reactant and uses mild reaction conditions to carry out the reaction. The synthesized Si QDs showed bright blue luminescence and good dispersibility in water and ethanol. The optical and structural aspects characterized the synthesized Si QDs. This low-temperature and facile synthesized method are suitable for large-scale production, and the obtained QDs can be further incorporated into optoelectronic devices.

3.1 Si QDs synthesized routine

Nitrogen gas was aerated through the right neck before the reaction and throughout the synthesis process to maintain an oxygen-free environment. At the same time, a stirring controller connected to the mantle and a PID controller was used to produce the required heating and stirring. One thermal couple was connected via the left neck to monitor the thermal input accurately. Silica beads are filled in the mantle to maintain uniform heat distribution. 2ml Si precursor was injected into the three-necked flask, which was mounted on the mantle, mixed with 8ml solvent to start the hydrolysis reaction, keep stirring until the solution becomes clear and homogeneous, and dissolved 0.450g L-AA into water. The temperature effect is under-examined, injected the L-AA lentamente,

and gradually increased the temperature. Reacted 25mins and cooled down to extract the product, followed by the dialysis process (Sigma-Aldrich, molecular weight cut-off 1kDa) to eliminate the unreacted reactants and impurities. Dialysis for 20h and purify the QDs following a 20nm filter to remove the aggregated QDs and store the Si QDs in the fridge for further use.

3.2 Si QDs characterization methods

- Photoluminescence (PL) measurement was carried out with the fluorescence spectrometer (Edinburg instruments, USA). The light source for excitation is a 450W Xeon lamp.
- The QDs lifetime decay results were measured by the same spectrometer with a 375nm excitation wavelength pulsed LED source (Frequency= 5MHz, pulse width=943.3 picoseconds, Edinburg, USA) and analyzed by the time-correlated single-photon counting (TCSPC) method. Decay Data was processed with fluorescence analysis software technology (FAST) software (Edinburg instrument, USA).
- The size and crystallinity of the QDs are analyzed by the high-resolution transmittance electron microscope (HRTEM, ZEISS LIBRA 200 FE, Germany). Further QDs size distribution was processed by software Image J.
- Fourier transform infrared (FTIR) spectra was collected by Vertex 70v (Bruker, USA) and were used to collect the functional group data. Si QDs were drop casted on the KBr substrate.
- X-ray photoelectron spectroscopy (XPS, Thermo Fisher Scientific, USA) was used to measure QDs surface element composition and bond element.

3.3 Si QDs development and characterization.

3.3.1 Si QDs photoluminescence results

Reaction temperature, reaction time, and reductant concentration are the significant parameters that will influence the QDs' final size and structural composition. The temperature effect on the quantum dots growth was thoroughly investigated via Photoluminescence (PL) measurement, and the results are shown in fig.3-1. L-AA is a mild and green reductant, which will start to degrade from 85℃. Thus, we investigate the temperature range from 25 degree Celsius to 75 degrees Celsius with 10 degrees Celsius internal [45]. The formation of Si QDs followed by precursor hydrolysis in the solvent first, the -OH group will substitute for the -OCH3 group. Then water condensation process happens, which will form the Si-O-Si network. After adding the reductant L-AA, the silicon oxide network will be reduced, creating a Si nanocrystal core. At this stage, comparable small-size QDs formed in this nucleation stage. Afterward, Ostwald ripening process appeared on the stage. Small-size QDs decompose and redeposit on the larger nanocrystals. Carbon-based group and dehydroascorbic acid(DHA) ligand will attach to the Si QDs surface[46].

As depicted in fig.3-1, Si QDs reacted at 45℃ with the peak center located at 484 nm showing the highest PL intensity and emitted blue light under 365nm UV illumination. As the gradual temperature variation, the peak center shifts from 480nm to 505nm, which indicates the redshift happened as reaction temperature ramped, and the core size grew larger. The highest PL intensity was obtained at 45℃. Increasing temperature afterward will lead to a decrease in PL intensity, and redshift happened due to the rapid QDs growth and creating of more defects on the surface. Non-radiative emission becomes more dominant compared to the radiative transition. On the contrary, low-temperature 25℃ is insufficient to reduce the Si-O-Si network thoroughly and further propel

the Ostwald ripening process to obtain the high emission QDs. Then the mild temperature of 45℃ is the most optimal thermal condition and applied for further treatment, which is very cost-effective.

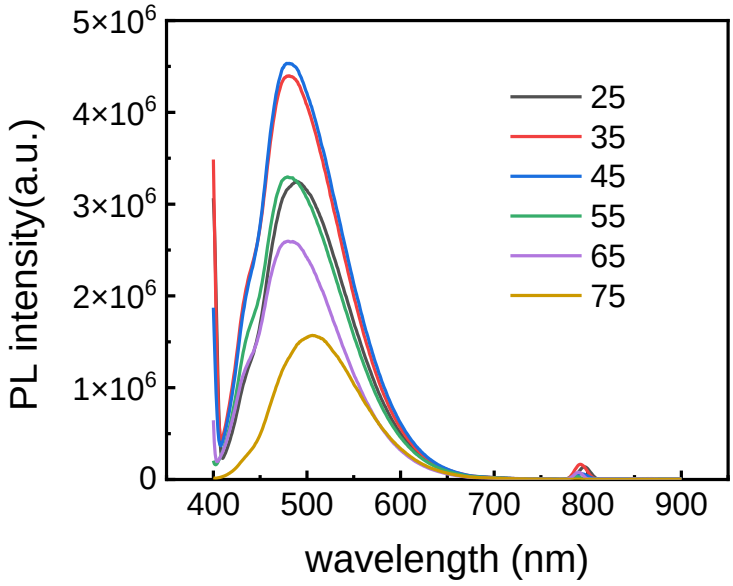

Figure 3-1 temperature effect on Si-QDs photoluminescence (PL) emission intensity.

In addition, the concentration effect of the reactant L-ascorbic acid was investigated under the optimized temperature of 45 degrees Celsius. The PL emission results are illustrated in fig.3-2. The role of L-AA is to cleavage the Si-O-Si network and form the Si nanocore. The peak centers for 0.450g and 0.900g L-AA are located at 490nm and 520nm. A considerable three folds of PL intensity suppression and redshift could be observed, which indicated the excess L-AA was added for the 0.900g condition. The unreacted L-AA remained in the solution and tended to attach to the Si QDs surface, acting as impurities to trap the Si QDs, which will hinder the QDs' radiative transition process and restrain the photoluminescence emission intensity. However, the Si QDs obtained with more L-AA added emit green light, which achieves slightly color-tunable from the previous cyan/blue color emission. The light emission under a UV lamp is shown in the inset, and

a brighter luminescence can be observed for the less reductant concentration sample. Further dialysis and filtration processes can be applied to purify the unreacted reactant and enhance the PL intensity.

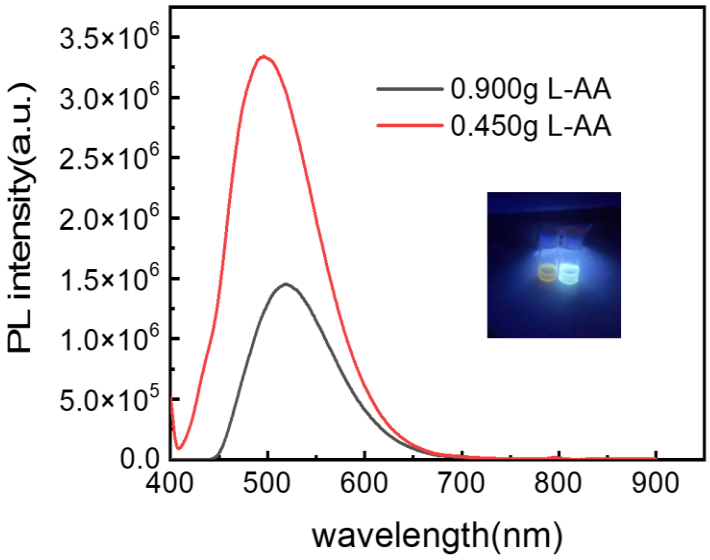

Figure 3-2 reductant concentration effect on Si-QDs photoluminescence (PL) emission intensity, inset shows light emission under 365nm UV lamp (left-hand side is the 0.900g L-AA sample, right is the 0.450g L-AA sample).

The thermal couple and Mantle achieve real-time temperature monitoring and thermal transfer. Meanwhile, the stirring also helps maintain the solution homogeneously and better control the Si QDs growth. However, one of the weaknesses of the bottom-up methods is the size distribution is hard to control precisely, which needs further size purification[47]. Fig3.3(a) compares the filtration effect and dialysis effect on PL intensity; deploying the dialysis process for 20h will remove the impurities to the buffer solution and leave the majority QDs in the dialysis bag, which enhances the PL intensity. A small amount of Si QDs was detected in the dialysis solution through PL measurement. PL intensity equals approximately 2.5% of the original Si QDs

emission level. Longer time (more than 72h) dialysis may cause more QDs diffusion to the dialysis solution and unstable surface ligand attachment, which will form the clumpy sediment due to the ligand stripped and reduce the PL intensity. Besides, using the filter will percolate the aggregation particles, and the QDs size below 20nm will remain in the solution. The PL intensity decrease is explainable afterward due to losing the gathering QDs.

The light blue color emissions of the purification samples and the untreated sample illuminated under 365nm UV light in the dark were shown in Fig.3-3(a) inset. Brighter light can be observed after purification, which proves the necessity of dialysis and filtration. In addition, centrifuging the Si QDs with 6000rpm for 5mins can validly enhance the PL emissions. The results before and after centrifuge are shown in Fig.3-3(b), and more than 50% PL increment could be observed. The possible mechanism for the PL improvements is that centrifuge helps to separate the aggregated Si QDs and exposure more light absorption sites on the separated Si QDs surface, proving the centrifuge process's usefulness.

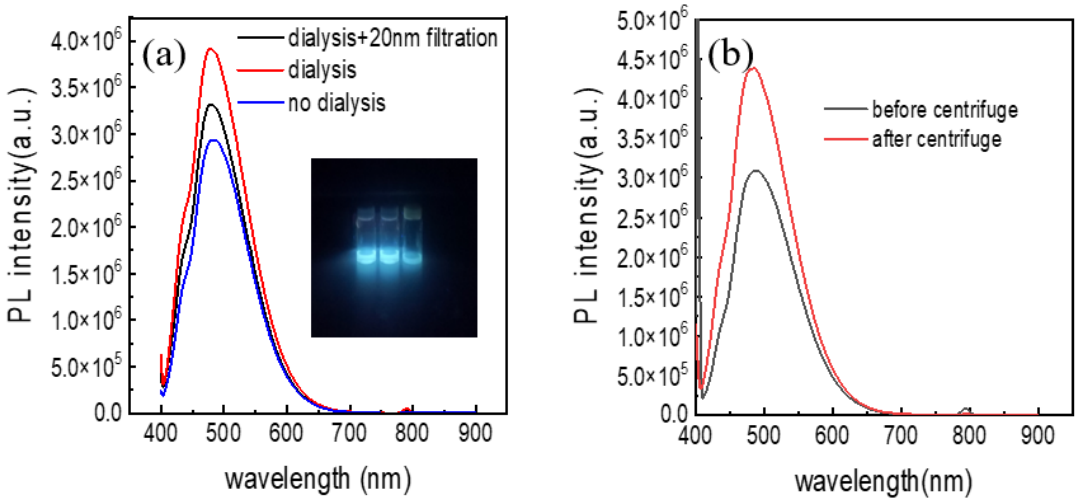

Figure 3-3(a). dialysis effect on Si QDs PL intensity and the inset shows QDs luminance under UV lamp (Left: after dialysis and filtration. Middle: after dialysis without filtration. Right: without dialysis and filtration.) (b) centrifuge effect on PL emission density.

After storing for two weeks, the PL result illustrated in fig.3-3(b), the peak center has only 3nm blueshift and maintains the same level of PL intensity instead of PL degradation, which also indicates the relative stability of the water-based Si-QDs. The increase of the PL intensity is due to the mild reaction conditions and the reversibility of green reductant L-AA; unreacted precursors are slowly reacting during the 2-week storage time and form small QDs. Due to the low temperature in the fridge and insufficient thermal energy to support the growth of the newly created small-size Si QDs, which causes the peak blueshift accompanies the stronger PL intensity emission.

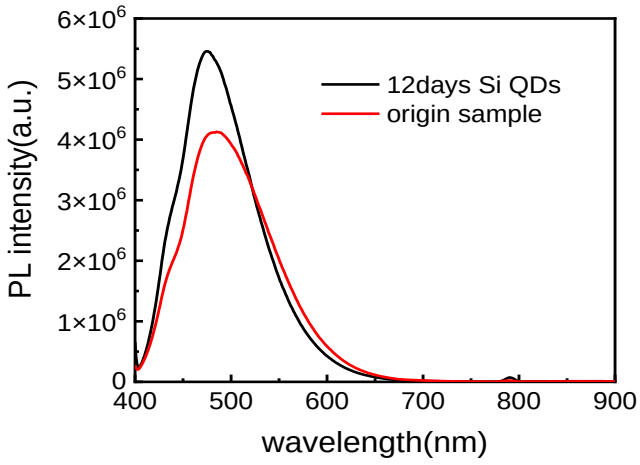

Figure 3-4. PL intensity comparison between Si QDs storage for 12 days and the fresh synthesis sample.

Figure 3.5(a) illustrates the PL decay curve of the water-based Si QDs, the decay curve was analyzed via tail distribution fitting in the software Fast, and the distribution components are

shown in Table 3-1. Shorter lifetime τ from peaks one and two are associated with the surface trap states, and the longer lifetime from peak three is related to internal defects [5]. F stands for the contribution fraction, as B is the pre-exponential fraction. The dominant lifetime with the largest f value for the Si QDs is 0.847ns. The further ligand exchange process can passivate the surface and extend the Si QDs lifetime effectively.

Table 3-1. Decay lifetime curve distribution components.

Peak number	B	f	$\tau(ns)$	T(ns)	Std $\tau(ns)$
1	32544	70	0.847	0.823	0.269
2	4208	27	2.541	2.674	0.401
3	113	2	9.905	9.980	0.393

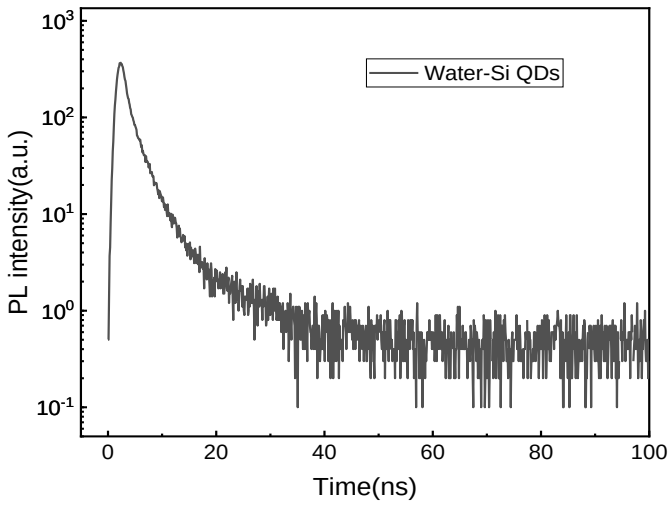

Figure 3-5. Si QDs Time-resolved lifetime decay.

3.3.2 Si QDs film deposition and PL measurements.

Solid-phase Si QDs film uniformity and photoluminescence were examined for further device application. Fig.3-5 illustrates the PL property of the Si QDs drop-casting film on ITO glass. The peak intensity and location are very consistent with the solution-phase Si QDs and proved the film owned the ability of light absorption. The illumination under UV showed the film is continuous and uniform due to the film crystallization. This QDs film meets the fundamental requirements of optoelectronic device application.

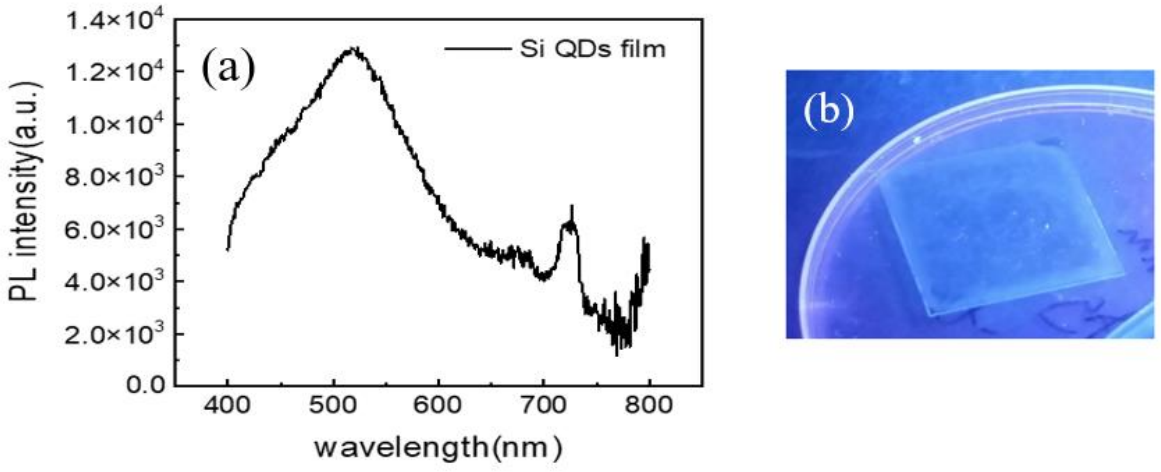

Figure 3-6(a). PL intensity of Si QDs drop-casting on ITO coated glass. (b) film illumination under the 365nm UV lamp in the dark.

3.3.3 Si QDs composition

XPS measurements are carried out to determine the Si QDs surface element composition and bond element. Fig 3-4(a) and (b) demonstrated the XPS results of Si QDs group elements and the silicon bonding on the core. The peaks located at 198eV, 284 eV, 398eV, 530.5eV,1072eV in fig.3-4(a) are corresponding to element Si, C, N, Na, O, respectively. Most Sodium, oxygen, and nitrogen elements originate from the dialysis buffer solution during the purification process.

Silicon and carbon are from the Si precursor and L-AA. QDs composition could be analyzed from Si 2p spectra in fig 3-4(b); binding energy at 100.2eV (red curve) and 102.6eV (green curve) are attributed to Si-C, and Si-O, respectively[48]. Compared to Si-O: Si-C=3 in precursor, the ratio in Si QDs decreased dramatically. The possible mechanism is that L-AA reduced the hydrolyzed Si-O-Si bond and formed the Si nanocrystal cores, which cut off most of the Si-O bond and decreased the Si-O signal. Followed by the Ostwald ripening process, carbon-based elements and DHA reattach to the Si QDs surface as the ligands[46]. The decreasing amount of the Si-O-Si signal also verifies the happening of the reduction process.

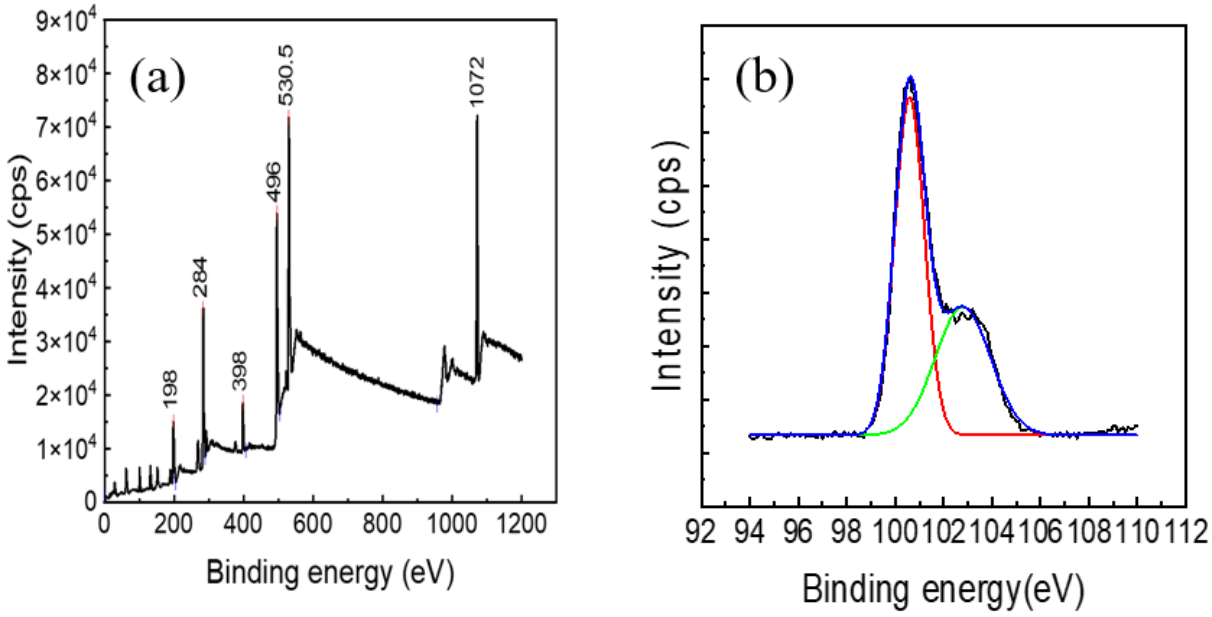

Figure 3-7. (a) XPS survey of Si-QDs after dialysis. (b) XPS spectrum of Si 2p orbital.

HRTEM was applied to analyze the size and crystallinity of the QDs, and images are shown in Fig. 3-5(a), (b), and (c), which can be used to analyze the QDs' crystallinity, size, and shape. The crystallinity and QDs sphere shape can be observed in Fig.3-5(a). The inset showed the diffraction pattern of the Si QDs. Fig.3-5(b) indicates good dispersity in water and QDs' spere

shape. Besides, no large aggregation is observed, which proves the filtration and dialysis process are beneficial for solution purification.

Meanwhile, the QDs size distribution was analyzed and counted through software image J, from Fig.3-5(c). Si QD diameters are calculated as 3.25±0.76nm, which is relatively uniform for this facile bottom-up method. In general, size control for the bottom-up method is challenging because the size will be highly affected by the pH, temperature, and solution uniformity[49]. Thus, it is essential to apply the filtration process after the one-pot synthesis to narrow down the size distribution. Size control is very significant for scale-up production and further optoelectronic application. However, to apply as the active layer in the photodetector, except for the uniform size distribution, the ligand attached to the surface also plays a significant role.

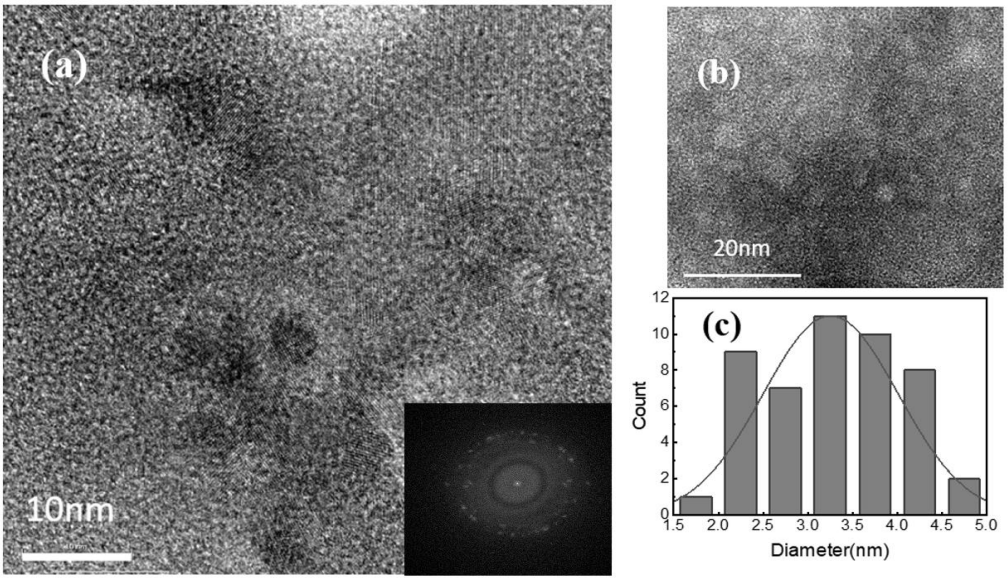

Figure 3-8(a) HRTEM image of Si-QDs, scale bar =10 nm, inset is diffraction pattern (b) HRTEM image of Si-QDs, scale bar=20nm (c) Si QDs size distribution count.

3.4 Summary

One facile and cost-effective method was developed in this chapter. The effects of the temperature, reductant concentration, and further purification process include dialysis, filtration, and centrifuge. A bright luminescent and non-toxic Si QDs with the size of 3.25±0.76nm were obtained; further quantum dots ligand effect will be discussed in the following chapters.

4. Si QDs ligand exchange and characterization

Si QDs-based optoelectronic device is of great interest because of their low toxicity, excellent light absorption ability, tunable bandgap, and various color emission. The main challenges of the device's efficiency development include poor film adhesion and low carrier transportability in the QDs layer. Researchers keep working on optimizing the QDs' structural properties and the device's other functional layer deposition to improve device performance. In addition, the ligand attached to the Si QDs plays a significant role in carrier transportation. The shorter ligand may cause more electronic state overlapping and decrease the energy barrier, further accelerating the electron transfer rate and improving the device's responsivity and the on-off ratio[50]. Compared to the traditional ligand washing and filtering methods, which can't remove the ligand thoroughly and need a complicated operation, one effective way to take place the undesired long ligand is called the ligand exchange process. The ligand exchange process mainly substitutes the long ligands with short ligands and includes solid phase and solution phase exchange, which execute the reaction when the QDs are in the film form or solution form. This chapter mainly focuses on Si QDs solution-based ligand optimization with MPA; modified Si QDs were characterized by optical and structural measurement.

4.1 Si-QDs solution-based ligand exchange

The ligand choice is critical and can be achieved by the ligand exchange process, and dangling bonds will be introduced afterward, forming mid-gap states. Film phase exchange can help to avert the QDs aggregation but suffers from the incomplete exchange issue, especially at the interface, which will negatively impact the charge injection or collection. Instead, the solution-phase ligand exchange process can substitute the previous ligand more thoroughly. The short side chain in MPA

ligand promotes the electronic coupling compared to the insulating-like long hydrocarbon chain as the long interdot distance will increase the tunneling barrier[51]

The Short side chain in 3-Mercaptopropionic acid (MPA) motivates it to be a remarkable candidate for the ligand exchange process. In this work, MPA was added to finalize the ligand exchange process, which substituted the long hydrocarbon side chain and passivates the QDs surface. The thiol-terminated structure enhances the radiative recombination process, extends more than 20% of Si-QDs lifetime, and promotes the photodetector response. In addition, thermal annealing of the solid-state QDs film can decrease the interdot distance and intensify the tunneling, increasing both dark current and photocurrent[52]. The annealing process can also help to suppress the C-H stretching, which indicates the removal of the organic residues in the film [53]. The Fourier transform infrared spectroscopy (FT-IR), and QDs-based device performance demonstrate the ligand exchange effect. This facile stepwise synthesis material can turn into a remarkable replacement for toxic Cd-based and Pb-based QDs.

4.2 Characterization methods

- Photoluminescence (PL) measurement was implemented after the ligand exchange with the fluorescence spectrometer (Edinburg instruments, USA). The light source for excitation is a 450W Xeon lamp.
- The QDs lifetime decay results were measured by the same spectrometer with a 375nm excitation wavelength pulsed LED source (Frequency= 5MHz, pulse width=943.3 picoseconds, Edinburg, USA) and analyzed by the time-correlated single-photon counting (TCSPC) method. Decay Data was processed with FAST software (Edinburg instrument, USA).

- Fourier transform infrared (FTIR) spectra was collected by Vertex 70v (Bruker, USA) and was used to collect the functional group data. The QDs film sample is prepared by drop-casting on the KBr substrate.
- The Ultraviolet-visible spectroscopy scanning measured the absorption of the QDs from 300nm to 800nm (UV-Vis, Shimadzu, Japanese)

4.3 Ligand exchange experimental procedure

One of the most dominant advantages of liquid-phase ligand exchange compared to solid-phased one is more controllable and can exchange ligands thoroughly. To better dissolve MPA in Si QDs solution, and withstand the difficulty of water-based film coating on the hydrophobicity surface of transparent electrode indium tin oxide (ITO), the solvent during Si QDs synthesis was changed to ethanol. 0.5ml MPA solution was added into 2ml purified Si QDs, sealed the cap, and sonicated for 60 mins to assist the ligand exchange process and alleviate QDs aggregation. Then, storage the modified Si QDs in a dark environment for two days to let the MPA ligand completely replace the original alkane ligands and attach them to the available site on the QDs surface. Color changing from light yellow to orange could be observed, indicating the ligand exchange happened. The Si QDs before and after ligand exchange are denoted as Ethanol-Si QDs and MPA- Si QDs, respectively.

4.4 MPA capped Si QDs characterization.

4.4.1 Chemical structural analysis of the ligand exchange

After the ligand exchange process, the long hydrocarbon chain attached to the QDs surface will be substituted by the shorter ligand origins from MPA. To verify the happening of the ligand exchange reaction, FT-IR measurements are employed to analyze the functional group absorbance and chemical change. The FT-IR results are shown in Fig.4-1(a) and (b). High-intensity vibration

in 2800-3000 cm^{-1} corresponds to the C-H stretching in Ethanol-Si QDs, which origins from long hydrocarbon chain stretch[20]. An apparent decrease of C-H stretching appeared, suggesting the long chain is replaced by the short ligands from MPA successfully. In fig. 4-1(b), stretching frequency between 480-490 cm^{-1} corresponds to the Si-S bond. After ligand exchange, the Si-S absorbance increases, proving the thiol-group origins from MPA attached to the QDs surface[54]. FT-IR results indicated the long ligand had been substituted by the new MPA ligand, followed by the implementation of the optical characterization to analyze the MPA-Si QDs' photoluminescence properties.

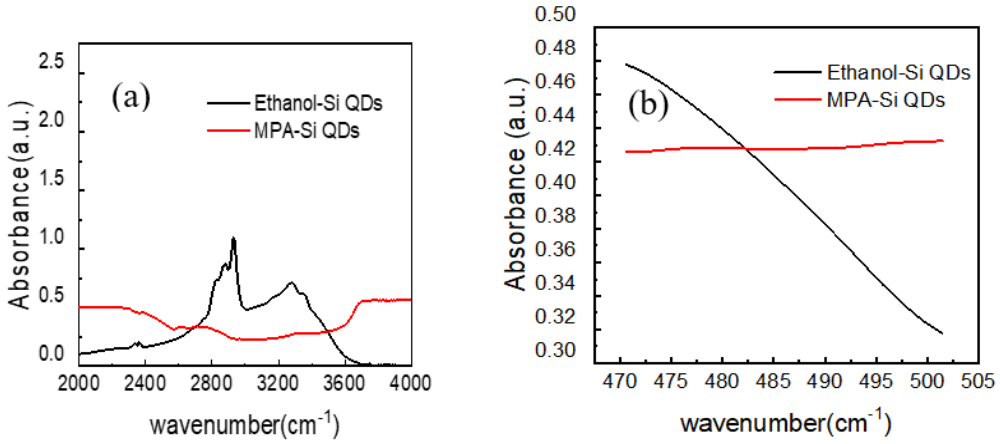

Figure 4-1(a) and (b) FT-IR results before and after ligand exchange

4.4.2 Optical photoluminescence and lifetime analyze

The PL results of Ethanol-Si QDs and MPA- Si QDs were compared in Fig.4-1(a). The peak redshift will influence the QDs' optical properties directly. After ligand exchange, the PL peak center shifts from 500nm to 520 nm, which emits green-blue and green light under a 365nm wavelength UV lamp, as shown in Fig.4-1(b), and solution color change could be observed. PL intensity also increased 20% afterward, originating from the MPA-passivating the unsaturated

surface state and enhancing the radiative combination. Besides, the mechanism for the exchange process is the new ligand getting through the original shell to replace the previous ligand, which will create radials and unsaturated QDs surface. MPA ligand is shorter and more chemically active than the long alkane chain and tends to recombine with the QDs core. Reattachment between the unsaturated QDs surface bond and the -SH bond will enhance the PL radiative emission and generate a slight redshift [55]. In addition, the PL emission redshift was due to the thiol-ligand attachment, and the MPA ligand exchange process will bring in the partly radiative mid-gap state due to the surface modification [56].

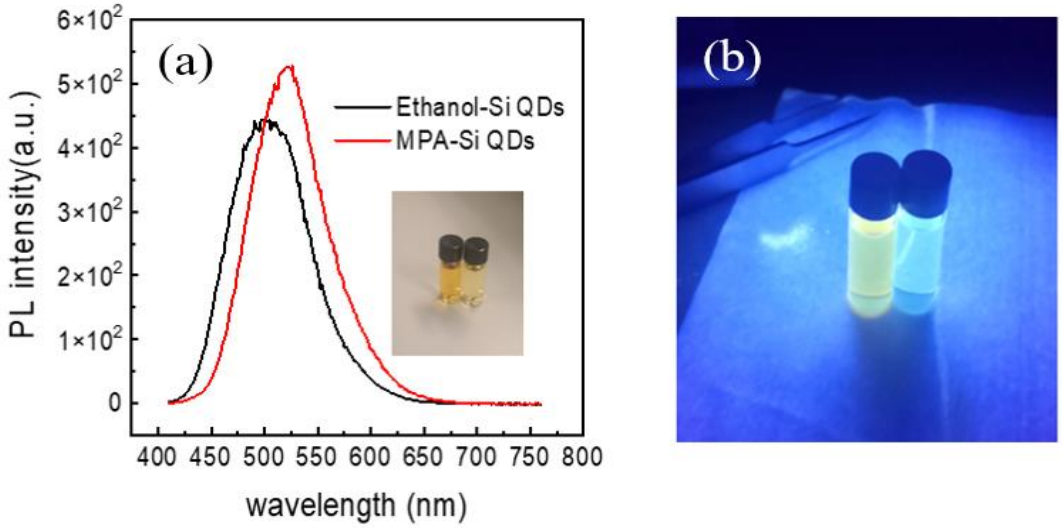

Figure 4-2(a) PL intensity of Si -QDs before and after ligand exchange, inset left sample is the MPA-Si QDs, the right sample is the Ethanol-Si QDs (b)Si-QDs under UV illumination, left: MPA-Si QDs. Right: Ethanol-Si QDs.

In order to investigate the effect of the solvent and ligand on the electronic process, fluorescence decay measurements were carried out. Fig.4-2 illustrates the photoluminescence decay curve of three kinds of Si QDs with various solvents and ligands. Data was analyzed in

FAST software and fitted with a distribution curve. As the detailed distribution components are listed in Table 4-1, the dominant lifetime for water-based Si QDs, ethanol-based Si QDs, and MPA-Si QDs are 0.85ns,1.04ns, and 1.26ns, respectively. Lifetime increased by more than 20% and 45% compared to the previous two non-ligand exchange processes. In addition, the f value of the long-lived decay time around 10's nanoseconds for MPA is the longest among these three kinds of Si QDs, which is 10.42 compared to the value of 4.82 and 2.83.

Meanwhile, the longest decay time value is 12.441ns compared to the lower value of 10.027ns and 9.905ns for non-ligand exchange Si QDs, which indicates organic solvent ethanol and MPA ligand can enhance the QDs' lifetime efficiently. Because of the change of the solvent dielectric constant and the carrier trapping enhancement by the MPA ligand[57]. Meanwhile, the thiol group effectively extends the intra-band relaxation time[58].

Besides, the free-carrier lifetime in the optoelectronic device is consistent with the QDs decay lifetime and provides suitability for device application. The longer lifetime is achieved through the MPA ligand attached to the QDs surface available site and benefits to passivate the surface defects [59]. The higher PL emission intensity and longer PL decay lifetime can prove that MPA-QDs are less defective[21]. Further, the optimized MPA-Si QDs will be applied to the planar photodetector device.

Table 4-1. Decay lifetime curve distribution components of Water-based QDs, Ethanol-Si QDs, and MPA-Si QDs.

Water-based Si QDs		Ethanol-Si QDs		MPA-Si QDs	
f	τ(ns)	f	τ(ns)	f	τ(ns)
70.01	0.847	80.71	1.044	62.29	1.257
27.16	2.541	14.47	3.564	27.29	3.617
2.83	9.905	4.82	10.027	10.42	12.441

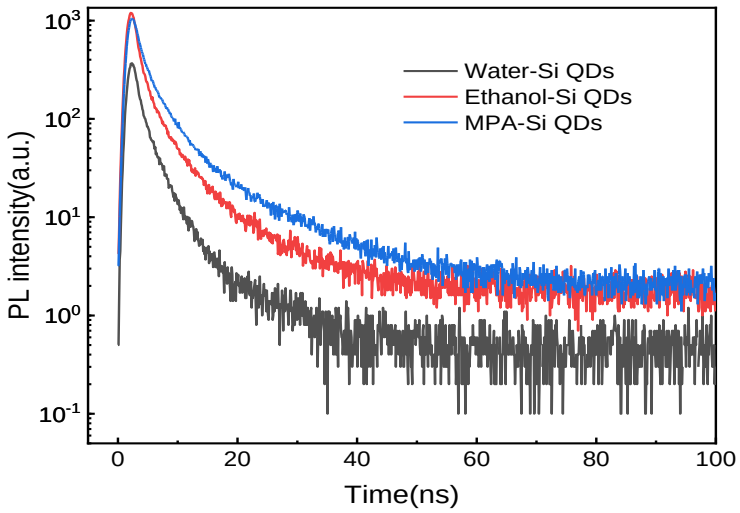

Figure 4-3. fluorescent decay curve of water-based Si QDs, ethanol-based Si QDs, MPA ligand Si QDs.

The UV-Vis measurement shown in Fig. 4-3 was carried out to determine the light absorbance of the Si QDs. The higher absorbance for the MPA-Si QDs is due to shorter interdot distance and

stronger electronic coupling[60]. And Stokes shift could be observed in both samples. The PL intensity increased after ligand exchange, consistent with the higher absorbance in Fig. 4-4. at 395nm, the higher absorbance for MPA-Si QDs in the lower energy range (450nm-500nm) is due to the creation of the radiative mid-gap state[56].

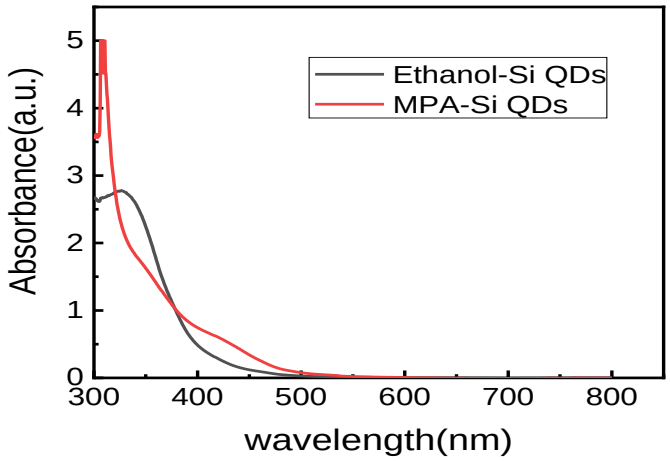

Figure 4-4. UV-Vis spectrum of Si QDs before and after ligand exchange.

To test the stability of the MPA-capped Si QDs in ethanol after more than two months of storage, PL emission measurement was implemented and shown in Fig.4-5. Compared to the fresh MPA-Si QDs, the PL peak center of 75 days MPA- Si QDs located at 520nm doesn't have any blue or red shift, which emits green light under UV illumination. The PL intensities are maintained at the same order of magnitude with acceptable growth, which proves the excellent stability of MPA-Si QDs in ethanol and the remarkable passivation effect of the MPA ligand. The ligand exchange Si QDs are appropriate to apply to large-scale production without worry about the QDs luminescence degradation after a long time of storage.

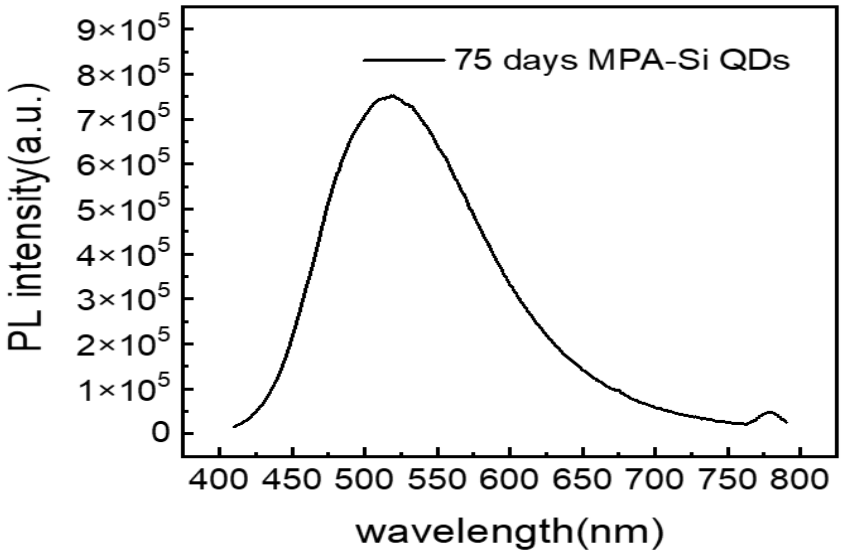

Figure 4-5. PL emission spectra for 75 days MPA- Si QDs.

4.5 summary

In this chapter, a detailed ligand exchange process with shorter ligand MPA was investigated, and FT-IR results proved the long hydrocarbon chain was replaced by MPA successfully. Further, the MPA-Si QDs were characterized by optical aspects. PL enhancement and redshift could be observed due to the thiol-group reattachment creating the mid-gap state and better passivation on surface dangling bonds. Besides, the MPA-Si QDs showed a longer decay lifetime than the non-ligand exchange Si QDs, which is beneficial for the device application. Further, the Si QDs photodetector device performance will discuss in chapter 5.

5. Si QDs photodetector fabrication and characterization

Quantum dots are one of the most promising materials for optoelectronic device applications because of their excellent light absorption and tunable light emission. However, it requires meticulous fabrication and consistent material polarity, to avoid the poor photo response from the nanometer-level thickness functional layer nonuniformity or film adhesion issues in QDs-based photodetector. This chapter focus on the Si QDs planar photodetector design and light response measurement. Device performance is characterized by the I-V measurement under dark and UV conditions. The front part of this chapter focuses on the device that fabricated the water-based non-ligand exchange Si QDs, as the rest was concentrated on the MPA-ligand Si QDs performance. A great improvement was observed for the ligand exchange QDs-based photodetector, which proves the ligand effect's significance on photodetector performance.

5.1 Si QDs photodetector

QDs are promising materials that can be applied in solar cells, LEDs, and transistors with their high light absorption in a broad light range. They can be processed through low-cost coating methods, such as spin coating, drop-casting, and dip coating, which can be applied in large-scale production and generate significant interest. In quantum dots, the transition between the discrete electronic states will happen after absorbing the photons with energy larger than the bandgap [7]. The photodetector is an optoelectronic device that converts optical signals to electrical signals after the device absorbs light. Carriers move and extract through the external electric bias and enhance the current. The change in the current compared to the dark situation can be used to reflect the optical input, called the photodetector. Its wide application attracts many researchers to investigate. The carrier transport in the solid QDs film is via tunneling, and the ligand barrier height highly

influences the tunneling rate (equation 5.1). ΔE and Δx are ligand-dependent energy barrier height and width. Lowering the energy barrier height can enhance the tunneling rate exponentially[7].

$$\Gamma \sim \exp\{-(2m^{*}\Delta E/\hbar)^{\frac{1}{2}}\Delta x\} \quad (5.1)$$

The ligand attached to the QDs surface can affect the interdot distance and interaction between neighboring particles. Shrinkage of the interdot distance will contribute to overlapping wave function [51]. The long organic side chain will act as a high energy barrier and hinder carrier movement. However, enough length ligand is essential to maintain the colloidal quantum dots' solubility and stability in the solvent[21].

Carrier lifetime will determine the photoconductive gain of the photodetector, as trap stats exist near the conduction band and the valence band can trap holes or electrons. The other type of carriers can circulate in the circuit till recombination or collected by the electrode, which helps to extend the free carrier lifetime and enhance the photocurrent[39]. In addition, the trapped minority carrier will be released gradually and contribute to the photocurrent, slowing down the photocurrent dropping time after removing the light input. In other words, the trap state can extend the carrier lifetime but limit the photo-response rate. The device fabricated in this work is measured in a sealed chamber to ensure the dark environment and one UV light source mount on the measurement stage and are controlled via the switch outside the chamber without disturbing the measurement environment. The ratio of the dark and illumination I-V characterization can be used to justify the response of the photodetector device.

Characterization methods

- Cyclic- voltammetry(C-V) can be carried out through the CHI600E electrochemical analyzer (CH Instruments, USA), which can determine the highest occupied molecular orbital (HOMO) and lowest unoccupied molecular orbital (LUMO) value. Ferrocene with known E_{HOMO} =

-4.8eV acted as reference material, and two platinum electrodes served as the counter and working electrode. Ag/AgCl was used as the reference electrode, and 0.1M tetrabutylammonium hexafluorophosphate was the electrolyte.

- Si QDs-based photodetector devices were measured with the Agilent 4155c semiconductor parameter analyzer (Axiomtest, USA) connected to a 2-point-probe station in a sealed black chamber. A UV lamp is mounted on the measurement stage and can be controlled through the switch outside the chamber without disturbing the device measurement. The external bias is provided by the power supply Agilent E3620a (Axiomtest, USA).
- DekTak 150 (Veeco, USA) was employed to perform the surface profilometry and rough thickness measurement.
- The scanning electron microscope characterized the functional film thickness and morphology in devices (SEM, Zeiss Ultra Plus, Germany). The cross-sectional device was prepared via the cleavage tool, and the sample surface was sputtered with 130s Ag thin film in advance to improve the samples 'conductivity and SEM image resolution.

5.2 Photodetector device fabrication

From the material chosen view, due to the perfect transparency, work function(4.73eV), and excellent conductivity, ITO-coated glass was employed as the bottom electrode for the photodetector device[61]. Si QDs act as the light-harvesting material to absorb the light. The band gap(2.8eV) and HOMO (-5.4eV) were calculated from the Cyclic voltammetry and UV-Vis result (Fig.4-4). The onset potential from Fig.5-1 is 0.6 eV, using ferrocene with known E_{HOMO} =-4.8eV as the reference material.

$$E_{HOMO} = - (4.8+E_{ox}) = -(4.8+0.6) = -5.4 \text{ eV} \quad (5.1)$$

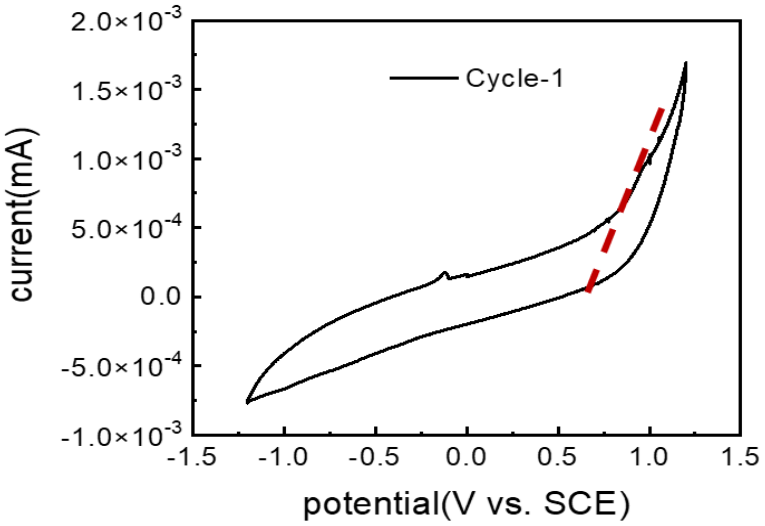

Figure 5-1 cyclic voltammogram of Si QD, using ferrocene as the reference.

Except for the material chosen aspect, functional layer coating methods also play a significant role in device fabrication. Thin-film coating methods mainly contain drop-casting, spin coating, dip coating, and doctor blading. Drop-casting is the simplest among these coating methods, and the solvent evaporation rate and temperature determine film uniformity. Film deposited thickness can range widely from one monolayer to several micrometers, determined by the material dispersity and crystallinity. The easy operation and low cost of drop-casting attract a lot of attention[62]. Compared to the simple drop-casting method, the thinner and more uniform film can be coated by the spin-coating method, the thickness of the film mainly depends on the rotation speed, and most of the solution will be ejected during substrate rotation. The lower rate at the beginning helps the solution spread over the device substrate, and higher speed rotation was employed to achieve the desired film thickness. Further, the last step uses a lower speed to help the solvent evaporation and improve the film uniformity. In addition, dip coating immerses the substrate in the solution with a slow pull rate, and the retrieved speed and solution viscosity determine the film thickness. The advantages of dip coating are highly repeatable and could obtain

a relatively uniform film. To thinner the film thickness, a lower withdrawal speed must be employed[62].

5.2.1 Planar ITO/Si QDs /Ag photodetector fabrication.

Firstly, wash the ITO glass with the following sequence: acetone, 2-propanol, and DI water. Si QDs were deposited through low-cost spin coating or the simplest drop-casting method. To improve the film uniformity, the comparison of the thermal annealing effect is involved and investigated. The Kapton tape covered a 2.2cm*0.25cm area at the edge to leave some bare ITO area for I-V measurement. Spin coating Si QDs film followed the procedure of 300rpm 20s +2000rpm 30s +500 rpm 10s, and drop-casting Si QDs was drizzled onto the substrate and dried overnight in the desiccator. Afterward, thermally annealing the QDs film at 200℃ on the hotplate for 10mins aim to shorten the interdot distance and improve the film attachment. 200-500nm thickness silver dot with 0.5mm diameter (Ag, work function=4.3eV) as the top contact is deposited through the e-beam evaporation system (Nanochrome, Intlvac Inc, Canada) in a 10^{-6} Torr base pressure environment. Covered by a shadow mask to control the deposit area, 100 rpm rotation is assisted in depositing the metal on the substrate evenly. The deposition rate is maintained at a lower rate(1.0 Å/s to 1.5 Å/s) to avoid Ag punching through the Si QDs film and touching the surface of ITO, which will cause severe device shorting issues during device operation [63].

5.2.2 Planar ITO/Si QDs /Ag photodetector device characterization

Water-based Si QDs acted as the sensitizing center to absorb the light and create the electron-hole pairs. When the electrons are captured, the photogenerated holes are free to circulate until collected by the electrode or recombined[7]. The Device structure and energy diagram are

illustrated in fig.5-2. The grey area is the bare ITO bottom electrode covered by the Kapton tape before Si QDs spin-coating or drop-casting for device measurement. And the yellow area is the QDs spread area, followed by silver electrodes deposited with a shadow mask, which is illustrated as the dark spots in fig5-2(a), as the device energy alignment diagram was shown in Fig.5-2(b). The electrons will flow to the Ag side as the holes will be collected by the ITO electrode. The asymmetric structural can helps the charge separation.

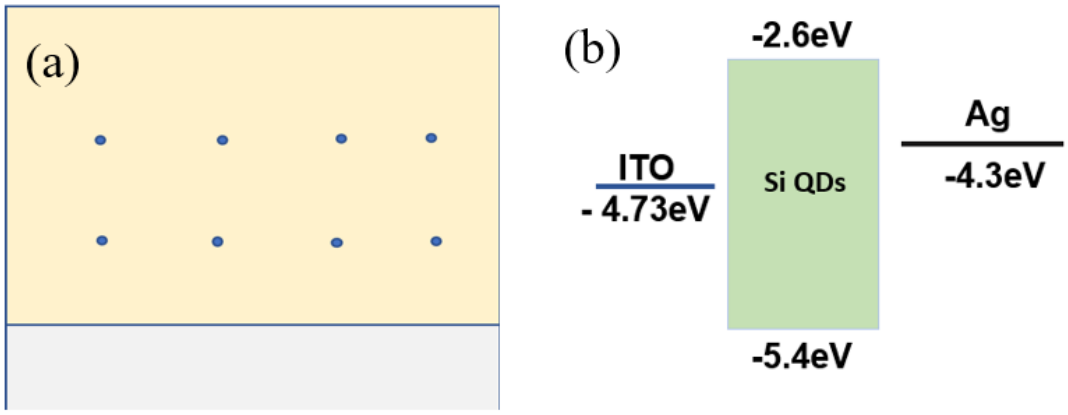

Figure 5-2(a) ITO/Si QDs/Ag photodetector device structure (b) ITO/Si QDs/Ag photodetector device energy diagram

Further, the device structure was characterized by the DekTak instrument and dark I-V system. The spin-coating and drop-casting film thickness measured by DekTak technology were around 400nm and 5-6 microns, respectively, and the top contact is 200nm-500nm depending on the requirements and deposition time. The relation between the current and external bias is shown in Fig.5-3(a). A linear ohmic shape current was obtained for the spin-coating sample. The dominant reason is the poor attachment between the hydrophobic ITO surface and water-based Si QDs during the film spin coating process[64]. The repulsion between the surface leaves some bare ITO

substrate areas and contact with the Ag electrode. The insufficient QDs film coverage leads to the shortening between the electrodes during the measurement.

As a comparison, QDs film coated with drop-casting method I-V characterization was illustrated in Fig.5-3(b). Instead of a linear ohmic shape current, a diode shape current was obtained. Meanwhile, the current order decreased from 10^{-2} A to 10^{-6} A, as water-based Si QDs were not very electrically conductive because of the insulating-like alkyl ligand attached to the surface[65]. A Thicker QDs layer was employed in the drop-casting device, which helps to lower the dark current. However, the QDs disorder and the long hydrocarbon ligand's poor carrier transportability contribute to the weak light response. The dark current and light current were $5.66 * 10^{-7}$ A and $7.73 * 10^{-7}$ A, respectively. The on-off ratio was defined as the ratio between photocurrent and dark current, and it is one of the most vital behavior factors to analyze photodetector sensitivity. The on-off ratio of the above device was depicted as 136.6%. The poor light response was due to most free carriers being incapable of being drawn to the electrode before recombination due to the carriers' short lifetime and the device's weak carrier transportation ability caused by the long side chain.

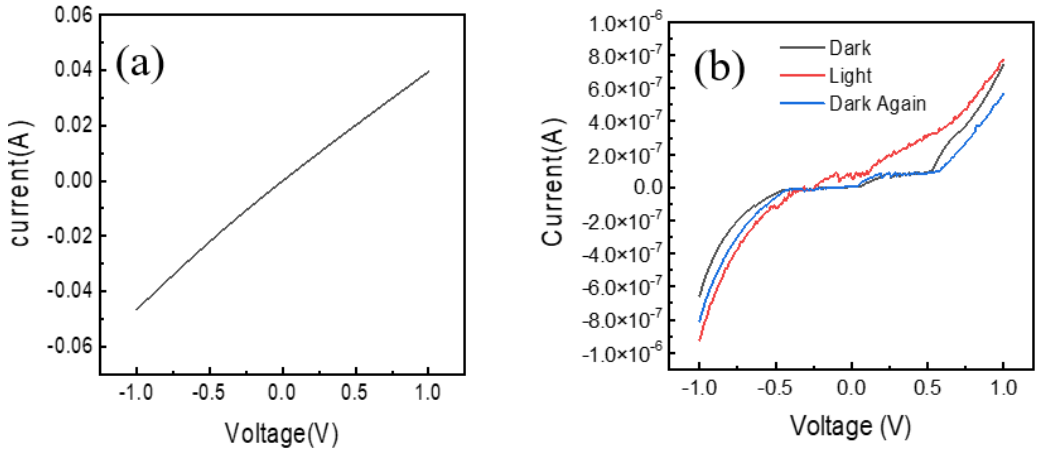

Figure 5-3(a) I-V characterization of spin-coating Si QDs device(b) I-V characterization of drop-casting Si QDs device.

5.2.2 ITO/Si QDs (65 ℃ annealing)/Ag photodetector

To further improve the uniformity and film order, the 10 mins low temperature 65 ℃ thermal annealing process was deployed without destroying the device structure, as thermal annealing can shorten the interdot distance and improve the film adhesion on the substrate. Other functional layers were fabricated following with previous procedure. The I-V characterization is shown in Fig5-4. Under the forwards bias, a light current of 3.68* 10^{-7} A was measured, and the dark current was 1.65 * 10^{-7} A, which stepped over the energy barrier under the forward bias. A higher on-off ratio of 223.0% was achieved compared to the non-thermal annealing sample, which mainly origins from more available carriers were transported and injected to the electrode under the UV illumination. In addition, the decreasing of the dark current of the thermal annealing sample also indicated fewer amounts of defects and a smaller leakage current. A smaller dark current is beneficial for weak optical input detection. However, no obvious response under reverse bias was

observed, which was ascribed to the small reverse bias was not sufficient to bend the interfacial band for carrier injection. Meanwhile, fewer carriers were generated at the ITO/Si QDs interface when the light was shining on from the Ag side. The light did not enhance the electron injection to ITO under reverse bias [66].

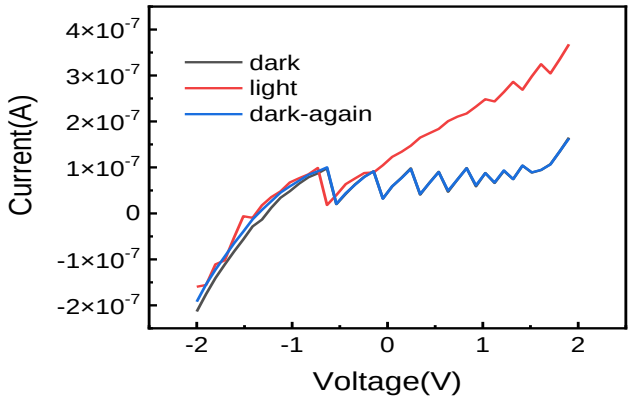

Figure 5-4. I-V characterization of thermal annealing Si QDs device.

5.3 MPA Si QDs Device fabrication and characterization

5.3.1 ITO/MPA-Si QDS/Ag planar photodetector

QDs with shorter MPA ligand performance were investigated to improve the device's performance. Existing of the partially delocalized mid-gap state(MGS) after ligand exchange can help to percolate the electrons and holes transport [67]. In addition, the stronger electronic state overlapping ascribed to the shorter MPA ligand was conducive to the carrier tunneling rate, which benefitted the optical response. SEM instrument was applied to study the morphology of the MPA-Si QDs film, as depicted in Fig.5-5(a), and a continuous and relatively uniform spin-coating QDs film could be observed. And shiny grains were introduced in the silver sputtering process during SEM sample preparation. The continuity and remarkable spreading of the film are due to the ethanol solvent, which restrains the repulsion force between the ITO/ Si QDs interface and

increases the wettability, contributing to better spreading on the ITO substrate. Besides, a cross-sectional SEM image of the MPA-Si QDs planar photodetector device was shown in Fig.5-5(b), 3.8μm thickness was made via the drop-casting method. Following by the 10 mins 180℃ thermal annealing process to improve film adhesion and shorten the interdot distance. Afterward, 200nm thickness Ag was evaporated as the top contact, which didn't show in the cross-sectional view. Further, this planar device will be characterized by the I-V measurement.

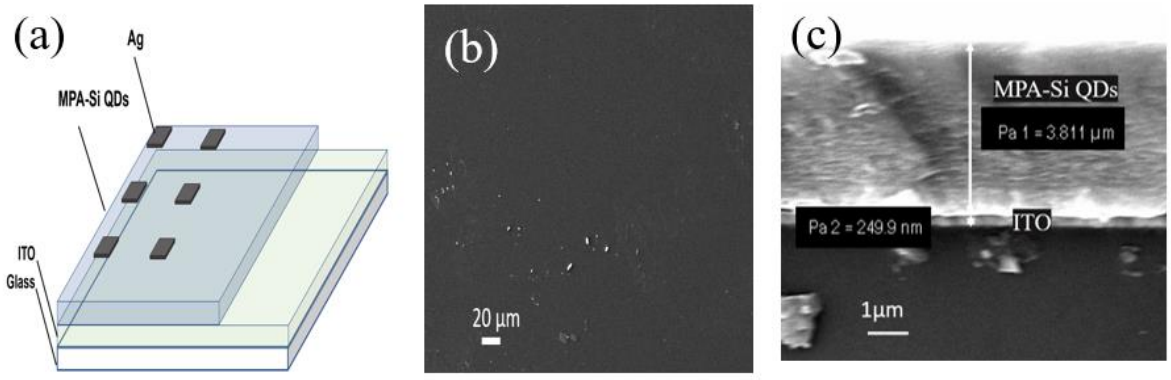

Figure 5-5 (a) Glass/ITO/MPA-Si QDs/Ag device scheme (b)SEM image of MPA-Si QDs film (c)SEM cross-sectional view of Glass/ITO/ /MPA-Si QDs /Ag photodetector Device.

The diode I-V curve changing corresponds to the light input shown in Fig.5-6; the device has a photo response after shining the UV light. As the dark current was 1.25* 10^{-5} A, and the light current increased to 2.49* 10^{-5} A, the on-off ratio was obtained as 199.2%, which was enhanced by the ligand exchange process; after receiving the light, the applied bias well separated the photocarriers created in the MPA-QDs. The second dark current returned to the original level, proving the current increase was caused by the only light variable. The explainable mechanisms behind this are through functionalizing the QDs surface by MPA ligands, the surface state was passivated as well as the carrier lifetime was extended. When the mid-gap state captured the

electrons during device operation, the photogenerated holes' lifetime was extended and free to transport via the valence band. Further carriers are collected by the electrode in the circuit, dedicated to the photocurrent generation[68]. Besides, the thermal annealing process can improve film adhesion and restrain contact resistance. Annealing provides energy to arrange the QDs in favorable positions and increase carrier mobility, contributing to the light current enhancement[69]. The increment of the dark current density compared to the water-based Si QDs was due to the ligand exchange process-induced trap states and smaller bandgap[70].

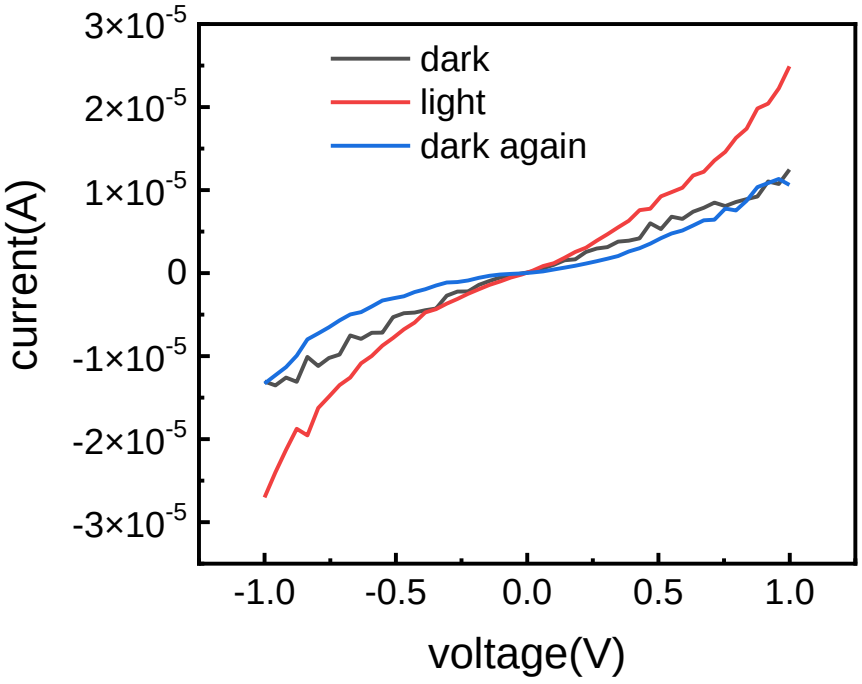

Figure 5-6.I-V characterization of Glass/ITO/ /MPA-Si QDs /Ag photodetector Device.

5.3.2 ITO/PEDOT: PSS/MPA-Si QDS/Ag planar photodetector

The hole transport layer (HTL) also plays an essential role in device performance and improves the photon response. Here we employed PEDOT: PSS as the HTL because of its high conductivity and suitable work function(about 5.0eV) to better assist the hole transport and extraction[71][72].

The heterojunction structure can effectively separate the carriers. Deposit the uniform PEDOT: PSS film with the following spin-coating procedure: 500rpm 30s+4000rpm 60s +500rpm 30s, followed by 120℃ thermal annealing for 5mins to improve the film uniformity and better attachment on 2.2cm*2.2cm ITO substrate, 320nm thickness PEDOT: PSS film was obtained. This planar structure scheme and energy diagram were illustrated in Fig.5-7(b), the shallow band of PEDOT: PSS can effectively transfer holes from MPA-Si QDs as well as block electron injection and recombination, meanwhile, electrons can be easier captured by the Ag electrode, this energy alignment can help the charge separation process.

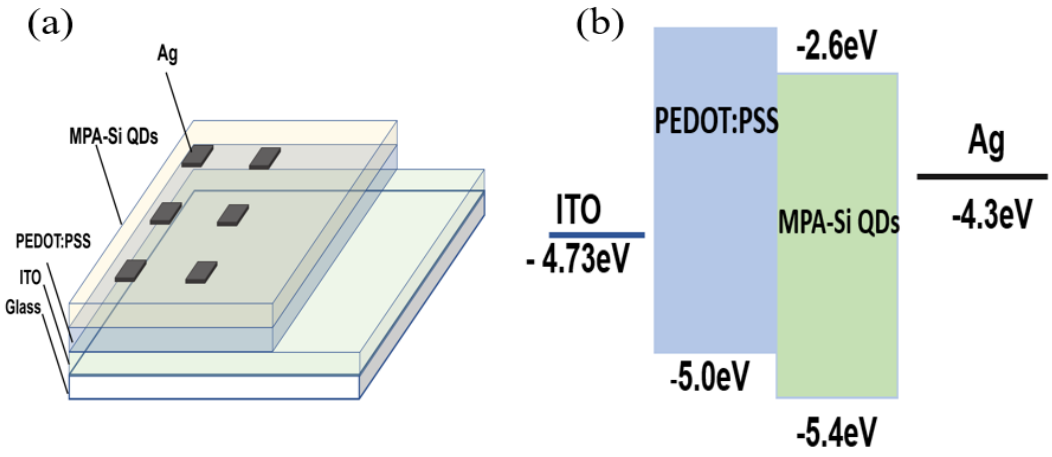

Figure 5-7 (a) Glass/ITO/PEDOT: PSS/MPA-Si QDs /Ag photodetector Device structure scheme. (b) Device energy band diagram.

The attachment of each functional layer plays an important role in photodetector performance, and poor attachment will introduce the shorting issue and poor carrier injection. To investigate the film morphology and attachment of each functional layer, the interface of each layer was characterized by the SEM instruments, and the cross-sectional view of ITO/PEDOT: PSS/MPA-Si QDS/Ag planar photodetector was depicted in Fig.5-8, a good attachment between

the MPA-Si QDs layer and PEDOT: PSS was demonstrated, which was good for the carrier injection, as well as a uniform 190nm Si QDs film was obtained through spin coating method, as the polar ethanol solvent helps the Si QDs spread well on the substrate, suppress the QDs aggregation and island shape particles formation.

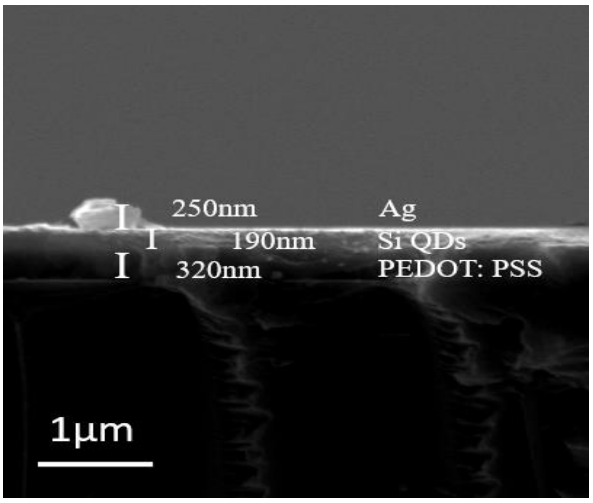

Figure 5-8. SEM cross-sectional view of Glass/ITO/PEDOT: PSS/MPA-Si QDs /Ag photodetector Device

5.3.3 I-V characteristics of planer /ITO/PEDOT: PSS/MPA-Si QDs /Ag photodetector

To deeply investigate the ligand effect on the photodetector performance, ITO/PEDOT: PSS/Si QDs/ Ag device was fabricated with Si QDs after ligand exchange. Fig.5-9 illustrated the I-V curve with the light on and off, and a second dark curve was measured to prove the current change origins from the light input. Measurement was carried out in a black chamber with a controllable UV lamp. For MPA-Si QDs-based devices, dark current and light current are $2.18*10^{-6}$A and $1.59*10^{-5}$A, respectively. The on-off ratio after ligand exchange was 729.4%, the highest among all fabricated devices, ascribed to the MPA-Si QDs' longer carrier decay lifetime and the heterojunction structure. PEDOT: PSS slightly lower highest occupied molecular orbitals (HOMO) provide excellent hole

transportability and enhance the carrier separation and collection. In addition, shorter ligands and longer lifetimes contribute to better carrier transportation and extend the time before carriers recombine to inject more carriers into the device I-V results also prove the necessity of ligand exchange. Besides, carrying the ligand exchange will create some new energy states and additional trap states. The surface trap state will capture the electrons or holes, and the other type of carrier will recirculate through the circuit and contribute to the photocurrent before recombining [7]. The mid-gap state was introduced during the ligand exchange process, enhancing the photocurrent by transforming energy from the traps to the charge transfer state[56]. Free carriers in the spin-coating thin film can be easily captured apart from recombination compared to the thick drop-casting film. There are several possible mechanisms behind the light current increasing compared to the drop-casting ITO/MPA-Si QDs /Ag. (I) the larger light current was ascribed to the smaller band gap induced by the in-gap states existing in the MPA-Si QDs[73]. (II) the lead into of the PEDOT: PSS layer can dope into the QDs at their interface. The excellent π-π stacking structure in PEDOT: PSS provided good conductivity to the QDs film and accelerated the charge transfer rate, which enhanced the light current effectively[74]. (III) ITO film may degrade during the dual thermal annealing of the QDs layer and PEDOT: PSS layer and UV exposure during measurement, which will lower the work function of the ITO and more carriers injection[75][76]. (IV) The film attachment between the ITO/PEDOT: PSS or PEDOT: PSS/ QDs could also happen, it induced current leaking, which needs further optimization.

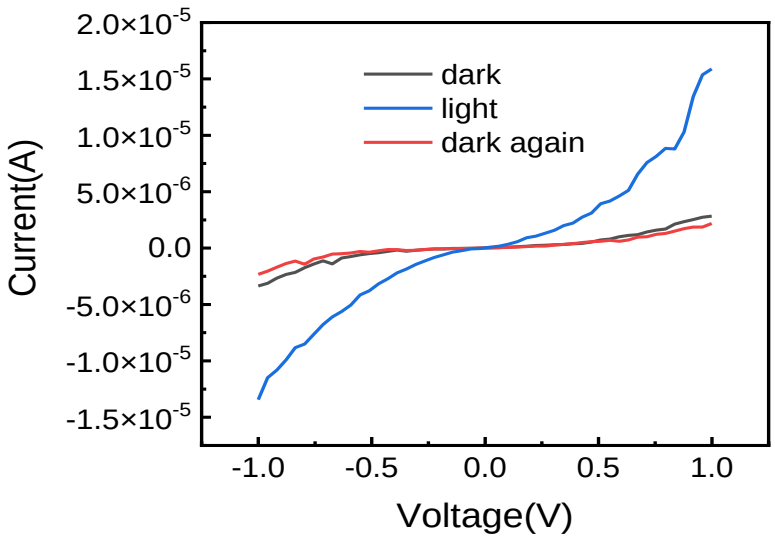

Figure 5-9. I-V result of MPA-Si QDs heterojunction planar device.

5.4 Summary

In summary, MPA-ligand QDs have the advantages of higher PL emission intensity, shorter sidechain compared to the original complex carbon chain, defects, and longer decay lifetime. These features are significant for optoelectronic device performance. Moreover, the water-based Si QDs and MPA-Si QDs were employed as the light-harvesting layer and applied to the planar ITO/ QDs/ Ag photodetector device. A comparison of the thermal annealing effect and the film coating methods was carried out. The thermal annealing process can suppress the QDs film disorder and shorten the interdot distance. MPA-Si QDs devices fabricated with different structures showed an excellent photo response to the light. The I-V results indicated that MPA-Si QDs-based photodetector conducts a better on-off ratio than the Si QDs without ligand exchange. Hole transport layer PEDOT: PSS and Si QDs formed heterojunction structures and contributed to a stronger photo response, which indicates the ligand exchange process can improve the device performance. Besides, MPA-Si QDs could be an excellent substitute for toxic Cd-based QDs.

6. Conclusions and outlook

6.1 Conclusions

This work presents a modified bottom-up Si QDs method and a developed photodetector device fabrication method. A low-temperature bottom-up was developed using AEAPTMS as the silicon precursor and L-AA as the reductant to produce the Si QDs. With the addition of the reductant, the Si-O-Si network was reduced to the Si core and further grown to the Si-QDs. Additionally, the temperature effect and further purifying effect were investigated, and the obtained Si QDs with a size distribution of 3.25±0.76nm showed bright blue under the UV lamp. This facile, low-cost method is suitable for scale-up production. Afterward, the long hydrocarbon chains originating from the water-based Si QDs will form a high energy barrier and hinder the carrier transport during device operation. To improve the applicability of Si QDs on photodetector devices, a solution-based assisted by the sonication MPA ligand exchange process was developed. A slight PL redshift and higher PL intensity were observed, ascribed to the surface passivation and in-gap states. After the ligand exchange, the lifetime of the Si-QDs increased by more than 20% and 45% compared to the non-ligand exchange ones. Besides, the MPA-ligand passivated Si QDs show fewer defects and better carrier transportability than the original QDs.

Further, these two kinds of Si QDs were applied on the planar device as the light-absorbing layer, ITO and Ag acted as the electrode, and the film spin coating and drop-casting methods effect were investigated. The spin coating water-based Si QDs without ligand exchange process showed shorting problems due to the poor attachment between QDs/ITO interface. The thermal annealing process involved solving this issue, and the film was coated by the drop-casting method. However, the planar device still showed a weak photo response towards the UV lamp. Further, the MPA-Si QDs were incorporated as a light-harvesting layer in the planar ITO/ PEDOT: PSS/ Si QDs/ Ag

photodetector device. It has a higher on-off ratio than the original Si QDs due to the less carrier transfer hindrance and the energy transfer from the mid-gap state; the photodetector with better performance also proves the necessity of the ligand exchange process.

6.2 outlook and future work

This section is the recommended expansion of this research topic. To narrow down the QDs size distribution and pure color emission for LED application, the size control of the Si QDs still needs to be optimized, which could be achieved in a higher-pressure production environment. With the higher-pressure growth condition, a more homogeneous solution could be obtained. In addition, other ligand exchange sources could be investigated, such as thioglycolic acid (TGA). With a shorter side chain compared to the MPA, which could be more advantageous to enhance the carrier transport in the photodetector device.

In addition, the heterojunction device could be further optimized, and introducing the electron transport layer (ETL) at the same time could improve the charge separation and device performance to a certain degree. Besides coupling Si QDs with some conductive material, such as graphene, the hybrid structure could also increase the on-off ratio significantly.

References

[1] T. D. Lee and A. U. Ebong, “A review of thin film solar cell technologies and challenges,” *Renew. Sustain. Energy Rev.*, vol. 70, no. September 2015, pp. 1286–1297, 2017, doi: 10.1016/j.rser.2016.12.028.

[2] D. Gielen, F. Boshell, D. Saygin, M. D. Bazilian, N. Wagner, and R. Gorini, “The role of renewable energy in the global energy transformation,” *Energy Strateg. Rev.*, vol. 24, no. June 2018, pp. 38–50, 2019, doi: 10.1016/j.esr.2019.01.006.

[3] A. Rao and R. H. Friend, “Harnessing singlet exciton fission to,” 2017, doi: 10.1117/2.1201203.004146.

[4] NERL, “Best Research-Cell Efficiencies: Emerging Photovoltaics,” *Best Research-Cell Efficiency Chart | Photovoltaic Research | NREL*. p. https://www.nrel.gov/pv/assets/pdfs/cell-pv-eff-em, 2022, [Online]. Available: https://www.nrel.gov/pv/assets/pdfs/cell-pv-eff-emergingpv-rev211214.pdf.

[5] Y. Zheng, B. Sadeghimakki, J. A. L. Brunning, E. M. Piano, and S. Sivoththaman, “Emission and Decay Lifetime Tunability in Less-Toxic Quaternary ZnCuInS Quantum Dots,” *IEEE Trans. Nanotechnol.*, vol. 20, pp. 525–533, 2021, doi: 10.1109/TNANO.2021.3090038.

[6] S. Miao and Y. Cho, “Toward Green Optoelectronics: Environmental-Friendly Colloidal Quantum Dots Photodetectors,” *Front. Energy Res.*, vol. 9, no. June, pp. 1–18, 2021, doi: 10.3389/fenrg.2021.666534.

[7] C. R. Kagan, E. Lifshitz, E. H. Sargent, and D. V. Talapin, “Building devices from

colloidal quantum dots," *Science (80-.).*, vol. 353, no. 6302, 2016, doi: 10.1126/science.aac5523.

[8] B. Sadeghimakki, Y. Zheng, N. M. S. Jahed, and S. Sivoththaman, "Synthesis of CIS Quantum Dots in Low-Temperature Regime: Effects of Precursor Composition and Temperature Ramps," *IEEE Trans. Nanotechnol.*, vol. 16, no. 4, pp. 659–666, 2017, doi: 10.1109/TNANO.2017.2703162.

[9] C. Lu, G. Chen, B. Yu, and H. Cong, "Recent Advances of Low Biological Toxicity Ag2S QDs for Biomedical Application," *Adv. Eng. Mater.*, vol. 20, no. 6, pp. 1–12, 2018, doi: 10.1002/adem.201700940.

[10] L. M. T. Phan *et al.*, "Synthesis of fluorescent silicon quantum dots for ultra-rapid and selective sensing of Cr(VI) ion and biomonitoring of cancer cells," *Mater. Sci. Eng. C*, vol. 93, no. July, pp. 429–436, 2018, doi: 10.1016/j.msec.2018.08.024.

[11] M. Isabirye, D. V. . Raju, M. Kitutu, V. Yemeline, J. Deckers, and J. Poesen Additional, "We are IntechOpen , the world ' s leading publisher of Open Access books Built by scientists , for scientists TOP 1 %," *Intech*, p. 13, 2012, [Online]. Available: http://dx.doi.org/10.1039/C7RA00172J%0Ahttps://www.intechopen.com/books/advanced-biometric-technologies/liveness-detection-in-biometrics%0Ahttp://dx.doi.org/10.1016/j.colsurfa.2011.12.014.

[12] S. Shen, B. Huang, X. Guo, and H. Wang, "A dual-responsive fluorescent sensor for Hg2+ and thiols based on N-doped silicon quantum dots and its application in cell imaging," *J. Mater. Chem. B*, vol. 7, no. 44, pp. 7033–7041, 2019, doi: 10.1039/c9tb01502g.

[13] C. Li *et al.*, “In vivo real-time visualization of tissue blood flow and angiogenesis using Ag2S quantum dots in the NIR-II window,” *Biomaterials*, vol. 35, no. 1, pp. 393–400, 2014, doi: 10.1016/j.biomaterials.2013.10.010.

[14] F. Gao *et al.*, “The synthesis of newly modified CdTe quantum dots and their application for improvement of latent fingerprint detection,” *Nanotechnology*, vol. 22, no. 7, 2011, doi: 10.1088/0957-4484/22/7/075705.

[15] M. Zhang, M. Wang, Z. Yang, J. Li, and H. Qiu, “Preparation of all-inorganic perovskite quantum dots-polymer composite for white LEDs application,” *J. Alloys Compd.*, vol. 748, pp. 537–545, 2018, doi: 10.1016/j.jallcom.2018.03.179.

[16] G. Mandal, M. Darragh, Y. A. Wang, and C. D. Heyes, “Cadmium-free quantum dots as time-gated bioimaging probes in highly-autofluorescent human breast cancer cells,” *Chem. Commun.*, vol. 49, no. 6, pp. 624–626, 2013, doi: 10.1039/c2cc37529j.

[17] Z. Ni, S. Zhou, S. Zhao, W. Peng, D. Yang, and X. Pi, “Silicon nanocrystals: unfading silicon materials for optoelectronics,” *Mater. Sci. Eng. R Reports*, vol. 138, no. April, pp. 85–117, 2019, doi: 10.1016/j.mser.2019.06.001.

[18] J. Wu, J. Dai, Y. Shao, and Y. Sun, “One-step synthesis of fluorescent silicon quantum dots (Si-QDs) and their application for cell imaging,” *RSC Adv.*, vol. 5, no. 102, pp. 83581–83587, 2015, doi: 10.1039/c5ra13119g.

[19] K. Dohnalová, T. Gregorkiewicz, and K. Kůsová, “Silicon quantum dots: Surface matters,” *J. Phys. Condens. Matter*, vol. 26, no. 17, 2014, doi: 10.1088/0953-8984/26/17/173201.

[20] Y. Zheng, B. Sadeghimakki, J. A. L. Brunning, and S. Sivoththaman, “Ligand exchange functionalization of cis quantum dots for cis/zno film heterojunctions,” *IEEE Trans. Nanotechnol.*, vol. 18, pp. 728–733, 2019, doi: 10.1109/TNANO.2019.2927951.

[21] X. Liu *et al.*, “Light-Emitting Diodes Based on Colloidal Silicon Quantum Dots with Octyl and Phenylpropyl Ligands,” *ACS Appl. Mater. Interfaces*, vol. 10, no. 6, pp. 5959–5966, 2018, doi: 10.1021/acsami.7b16980.

[22] F. Maier-Flaig *et al.*, “Looking inside a working SiLED,” *Nano Lett.*, vol. 13, no. 8, pp. 3539–3545, 2013, doi: 10.1021/nl400975u.

[23] M. Li, S. Ishihara, Q. Ji, M. Akada, J. P. Hill, and K. Ariga, “Paradigm shift from self-assembly to commanded assembly of functional materials: Recent examples in porphyrin/fullerene supramolecular systems,” *Sci. Technol. Adv. Mater.*, vol. 13, no. 5, 2012, doi: 10.1088/1468-6996/13/5/053001.

[24] B. Ghosh and N. Shirahata, “Colloidal silicon quantum dots: Synthesis and luminescence tuning from the near-UV to the near-IR range,” *Sci. Technol. Adv. Mater.*, vol. 15, no. 1, 2014, doi: 10.1088/1468-6996/15/1/014207.

[25] J. L. Heinrich, C. L. Curtis, G. M. Credo, K. L. Kavanagh, and M. J. Sailor, “Luminescent colloidal silicon suspensions from porous silicon,” *Science (80-.).*, vol. 255, no. 5040, pp. 66–68, 1992, doi: 10.1126/science.255.5040.66.

[26] T. H. Le and H. D. Jeong, “Characterization of band gaps of silicon quantum dots synthesized by etching silicon nanopowder with aqueous hydrofluoric acid and nitric acid,” *Bull. Korean Chem. Soc.*, vol. 35, no. 5, pp. 1523–1528, 2014, doi: 10.5012/bkcs.2014.35.5.1523.

[27] M. B. Gongalsky *et al.*, “Laser-synthesized oxide-passivated bright Si quantum dots for bioimaging,” *Sci. Rep.*, vol. 6, no. April, pp. 1–8, 2016, doi: 10.1038/srep24732.

[28] R. K. Baldwin, K. A. Pettigrew, E. Ratai, M. P. Augustine, and S. M. Kauzlarich, “Solution reduction synthesis of surface stabilized silicon nanoparticles,” *Chem. Commun.*, vol. 17, pp. 1822–1823, 2002, doi: 10.1039/b205301b.

[29] R. D. Tilley and K. Yamamoto, “The microemulsion synthesis of hydrophobic and hydrophilic silicon nanocrystals,” *Adv. Mater.*, vol. 18, no. 15, pp. 2053–2056, 2006, doi: 10.1002/adma.200600118.

[30] M. Abdelhameed *et al.*, “Tuning the Optical Properties of Silicon Quantum Dots via Surface Functionalization with Conjugated Aromatic Fluorophores,” *Sci. Rep.*, vol. 8, no. 1, pp. 1–10, 2018, doi: 10.1038/s41598-018-21181-8.

[31] C. S. Yang, R. A. Bley, S. M. Kauzlarich, H. W. H. Lee, and G. R. Delgado, “Synthesis of alkyl-terminated silicon nanoclusters by a solution route,” *J. Am. Chem. Soc.*, vol. 121, no. 22, pp. 5191–5195, 1999, doi: 10.1021/ja9828509.

[32] T. M. Atkins, A. Y. Louie, and S. M. Kauzlarich, “An efficient microwave-assisted synthesis method for the production of water soluble amine-terminated Si nanoparticles,” *Nanotechnology*, vol. 23, no. 29, 2012, doi: 10.1088/0957-4484/23/29/294006.

[33] S. Morozova, M. Alikina, A. Vinogradov, and M. Pagliaro, “Silicon Quantum Dots: Synthesis, Encapsulation, and Application in Light-Emitting Diodes,” *Front. Chem.*, vol. 8, no. April, pp. 1–8, 2020, doi: 10.3389/fchem.2020.00191.

[34] Z. Kang *et al.*, “Water-soluble silicon quantum dots with wavelength-tunable

photoluminescence," *Adv. Mater.*, vol. 21, no. 6, pp. 661–664, 2009, doi: 10.1002/adma.200801642.

[35] T. Nakamura, N. Koshida, Z. Yuan, and J. Otsubo, "High-yield green fabrication of colloidal silicon quantum dots by low-temperature thermal cracking of porous silicon," *APL Mater.*, vol. 8, no. 8, 2020, doi: 10.1063/5.0014206.

[36] K. Kůsová *et al.*, "Direct Bandgap Silicon: Tensile-Strained Silicon Nanocrystals," *Adv. Mater. Interfaces*, vol. 1, no. 2, pp. 1–9, 2014, doi: 10.1002/admi.201300042.

[37] B. Ghosh, T. Hamaoka, Y. Nemoto, M. Takeguchi, and N. Shirahata, "Impact of Anchoring Monolayers on the Enhancement of Radiative Recombination in Light-Emitting Diodes Based on Silicon Nanocrystals," *J. Phys. Chem. C*, vol. 122, no. 11, pp. 6422–6430, 2018, doi: 10.1021/acs.jpcc.7b12812.

[38] Y. Yu, C. E. Rowland, R. D. Schaller, and B. A. Korgel, "Synthesis and Ligand Exchange of Thiol-Capped Silicon Nanocrystals," *Langmuir*, vol. 31, no. 24, pp. 6886–6893, 2015, doi: 10.1021/acs.langmuir.5b01246.

[39] D. A. Hines, R. P. Forrest, S. A. Corcelli, and P. V. Kamat, "Predicting the Rate Constant of Electron Tunneling Reactions at the CdSe-TiO2 Interface," *J. Phys. Chem. B*, vol. 119, no. 24, pp. 7439–7446, 2015, doi: 10.1021/jp5111295.

[40] Y. Xu, S. Terada, Y. Xin, H. Ueda, and K. Saitow, "Ligand E ff ects on Photoluminescence and Electroluminescence of Silicon Quantum Dots for Light-Emitting Diodes," 2022, doi: 10.1021/acsanm.2c00811.

[41] J. Wang *et al.*, "Core/shell colloidal quantum dot exciplex states for the development of

highly efficient quantum-dot-sensitized solar cells," *J. Am. Chem. Soc.*, vol. 135, no. 42, pp. 15913–15922, 2013, doi: 10.1021/ja4079804.

[42] A. H. Ip *et al.*, "Hybrid passivated colloidal quantum dot solids," *Nat. Nanotechnol.*, vol. 7, no. 9, pp. 577–582, 2012, doi: 10.1038/nnano.2012.127.

[43] J. Huang *et al.*, "Improved performance of colloidal CdSe quantum dot-sensitized solar cells by hybrid passivation," *ACS Appl. Mater. Interfaces*, vol. 6, no. 21, pp. 18808–18815, 2014, doi: 10.1021/am504536a.

[44] T. Yu, F. Wang, Y. Xu, L. Ma, X. Pi, and D. Yang, "Graphene Coupled with Silicon Quantum Dots for High-Performance Bulk-Silicon-Based Schottky-Junction Photodetectors," *Adv. Mater.*, vol. 28, no. 24, pp. 4912–4919, 2016, doi: 10.1002/adma.201506140.

[45] P. Essodolom, B. Ekpetsi Chantal, M. Mamatchi, and A. Kousanta, "Effect of Temperature on the Degradation of Ascorbic Acid (Vitamin C) Contained in Infant Supplement Flours During the Preparation of Porridges," *Int. J. Adv. Res.*, vol. 8, no. 3, pp. 116–121, 2020, doi: 10.21474/ijar01/10605.

[46] D. Li *et al.*, "A facile synthesis of hybrid silicon quantum dots and fluorescent detection of bovine hemoglobin," *New J. Chem.*, vol. 43, no. 48, pp. 19338–19343, 2019, doi: 10.1039/c9nj05033g.

[47] B. Ali *et al.*, "Outstanding Graphene Quantum Dots from Carbon Source for Biomedical and Corrosion Inhibition Applications : A Review," 2021.

[48] B. Vincent Crist, "Handbooks of Monochromatic XPS Spectra Volume 1 - The Elements

and Native Oxides," *Handb. Elem. Nativ. Oxides*, vol. 1, no. September 2000, pp. 1–87, 1999, [Online]. Available: Handbooks of Monochromatic XPS Spectra.

[49] A. B. Cook and T. D. Clemons, "Bottom-Up versus Top-Down Strategies for Morphology Control in Polymer-Based Biomedical Materials," *Adv. NanoBiomed Res.*, vol. 2, no. 1, p. 2100087, 2022, doi: 10.1002/anbr.202100087.

[50] L. Zhou *et al.*, "Insight into the effect of ligand-exchange on colloidal CsPbBr3 perovskite quantum dot/mesoporous-TiO2 composite-based photodetectors: Much faster electron injection," *J. Mater. Chem. C*, vol. 5, no. 25, pp. 6224–6233, 2017, doi: 10.1039/c7tc01611e.

[51] D. V. Talapin, J. S. Lee, M. V. Kovalenko, and E. V. Shevchenko, "Prospects of colloidal nanocrystals for electronic and optoelectronic applications," *Chem. Rev.*, vol. 110, no. 1, pp. 389–458, 2010, doi: 10.1021/cr900137k.

[52] M. Drndić, M. V. Jarosz, N. Y. Morgan, M. A. Kastner, and M. G. Bawendi, "Transport properties of annealed CdSe colloidal nanocrystal solids," *J. Appl. Phys.*, vol. 92, no. 12, pp. 7498–7503, 2002, doi: 10.1063/1.1523148.

[53] V. J. Porter, S. Geyer, J. E. Halpert, M. A. Kastner, and M. G. Bawendi, "Photoconduction in annealed and chemically treated CdSe/ZnS inorganic nanocrystal films," *J. Phys. Chem. C*, vol. 112, no. 7, pp. 2308–2316, 2008, doi: 10.1021/jp710173q.

[54] S. Al-Dallal, M. Hammam, S. M. Al-Alawi, S. Aljishi, and A. Breitschwerdt, "Infrared spectroscopy of hydrogenated silicon-sulphur alloys prepared by glow discharge," *Philos. Mag. B Phys. Condens. Matter; Stat. Mech. Electron. Opt. Magn. Prop.*, vol. 63, no. 4, pp. 839–848, 1991, doi: 10.1080/13642819108205541.

[55] Z. Huang, Q. Zeng, Z. Bai, and S. Qin, “Regulating the Fluorescence Emission of CdSe Quantum Dots Based on the Surface Ligand Exchange with MAA,” *Polym. Adv. Technol.*, vol. 31, no. 11, pp. 2667–2675, 2020, doi: 10.1002/pat.4993.

[56] N. Zarrabi *et al.*, “Charge-generating mid-gap trap states define the thermodynamic limit of organic photovoltaic devices,” *Nat. Commun.*, vol. 11, no. 1, 2020, doi: 10.1038/s41467-020-19434-0.

[57] B. Omogo, J. F. Aldana, and C. D. Heyes, “Radiative and nonradiative lifetime engineering of quantum dots in multiple solvents by surface atom stoichiometry and ligands,” *J. Phys. Chem. C*, vol. 117, no. 5, pp. 2317–2327, 2013, doi: 10.1021/jp309368q.

[58] P. Guyot-Sionnest, B. Wehrenberg, and D. Yu, “Intraband relaxation in CdSe nanocrystals and the strong influence of the surface ligands,” *J. Chem. Phys.*, vol. 123, no. 7, 2005, doi: 10.1063/1.2004818.

[59] A. D. Andreev and E. P. O’Reilly, “Optical transitions and radiative lifetime in GaN/AIN self-organized quantum dots,” *Appl. Phys. Lett.*, vol. 79, no. 4, pp. 521–523, 2001, doi: 10.1063/1.1386405.

[60] A. Stavrinadis, D. So, and G. Konstantatos, “Low-Temperature, Solution-Based Sulfurization and Necking of PbS CQD Films,” *J. Phys. Chem. C*, vol. 120, no. 36, pp. 20315–20322, 2016, doi: 10.1021/acs.jpcc.6b05858.

[61] S. D. Nehate, A. Prakash, P. D. Mani, and K. B. Sundaram, “Work Function Extraction of Indium Tin Oxide Films from MOSFET Devices,” *ECS J. Solid State Sci. Technol.*, vol. 7, no. 3, pp. P87–P90, 2018, doi: 10.1149/2.0081803jss.

[62] J. Yang, M. K. Choi, D. H. Kim, and T. Hyeon, “Designed Assembly and Integration of Colloidal Nanocrystals for Device Applications,” *Adv. Mater.*, vol. 28, no. 6, pp. 1176–1207, 2016, doi: 10.1002/adma.201502851.

[63] M. Akbi and A. Lefort, “Work function measurements of contact materials for industrial use,” *J. Phys. D. Appl. Phys.*, vol. 31, no. 11, pp. 1301–1308, 1998, doi: 10.1088/0022-3727/31/11/003.

[64] S. Bayoudh, A. Othmane, F. Bettaieb, A. Bakhrouf, H. Ben Ouada, and L. Ponsonnet, “Quantification of the adhesion free energy between bacteria and hydrophobic and hydrophilic substrata,” *Mater. Sci. Eng. C*, vol. 26, no. 2–3, pp. 300–305, 2006, doi: 10.1016/j.msec.2005.10.045.

[65] M. Dasog, K. Bader, and J. G. C. Veinot, “Influence of halides on the optical properties of silicon quantum dots,” *Chem. Mater.*, vol. 27, no. 4, pp. 1153–1156, 2015, doi: 10.1021/acs.chemmater.5b00115.

[66] J. Miao, F. Zhang, M. Du, W. Wang, and Y. Fang, “Photomultiplication type narrowband organic photodetectors working at forward and reverse bias,” *Phys. Chem. Chem. Phys.*, vol. 19, no. 22, pp. 14424–14430, 2017, doi: 10.1039/c7cp01969f.

[67] Y. Zhang *et al.*, “Charge percolation pathways guided by defects in quantum dot solids,” *Nano Lett.*, vol. 15, no. 5, pp. 3249–3253, 2015, doi: 10.1021/acs.nanolett.5b00454.

[68] P. Nagpal and V. I. Klimov, “Role of mid-gap states in charge transport and photoconductivity in semiconductor nanocrystal films,” *Nat. Commun.*, vol. 2, no. 1, 2011, doi: 10.1038/ncomms1492.

[69] C. Y. Lee, Y. P. Kuo, P. Y. Chen, H. H. Lu, and M. Y. Lin, “Influence of annealing temperature on weak-cavity top-emission red quantum dot light emitting diode,” *Nanomaterials*, vol. 9, no. 11, 2019, doi: 10.3390/nano9111639.

[70] J. Qiu, B. Weng, L. L. McDowell, and Z. Shi, “Low-cost uncooled MWIR PbSe quantum dots photodiodes,” *RSC Adv.*, vol. 9, no. 72, pp. 42516–42523, 2019, doi: 10.1039/c9ra07664f.

[71] X. Huang, K. Wang, C. Yi, T. Meng, and X. Gong, “Efficient Perovskite Hybrid Solar Cells by Highly Electrical Conductive PEDOT:PSS Hole Transport Layer,” *Adv. Energy Mater.*, vol. 6, no. 3, pp. 1–8, 2016, doi: 10.1002/aenm.201501773.

[72] Z. Li *et al.*, “A low-work-function, high-conductivity PEDOT:PSS electrode for organic solar cells with a simple structure,” *Synth. Met.*, vol. 210, pp. 363–366, 2015, doi: 10.1016/j.synthmet.2015.11.006.

[73] N. Youngblood, C. Chen, S. J. Koester, and M. Li, “Waveguide-integrated black phosphorus photodetector with high responsivity and low dark current,” *Nat. Photonics*, vol. 9, no. 4, pp. 247–252, 2015, doi: 10.1038/nphoton.2015.23.

[74] E. Hosseini, V. Ozhukil Kollath, and K. Karan, “The key mechanism of conductivity in PEDOT:PSS thin films exposed by anomalous conduction behaviour upon solvent-doping and sulfuric acid post-treatment,” *J. Mater. Chem. C*, vol. 8, no. 12, pp. 3982–3990, 2020, doi: 10.1039/c9tc06311k.

[75] R. Schlaf, H. Murata, and Z. H. Kafafi, “Work function measurements on indium tin oxide films,” *J. Electron Spectros. Relat. Phenomena*, vol. 120, no. 1–3, pp. 149–154, 2001, doi: 10.1016/S0368-2048(01)00310-3.

[76] J. Kim, S. Shrestha, M. Souri, J. G. Connell, S. Park, and A. Seo, “High-temperature optical properties of indium tin oxide thin-films,” *Sci. Rep.*, vol. 10, no. 1, pp. 1–8, 2020, doi: 10.1038/s41598-020-69463-4.